Supplementary Information (SI) for Chemical Science.
This journal is © The Royal Society of Chemistry 2026

SUPPORTING INFORMATION

Beyond the Three-State Picture: When Higher-Lying Excited States Become Quantitatively Indispensable

Yue He, Daniel Escudero*

Quantum Chemistry and Physical Chemistry Division, Department of Chemistry, KU Leuven, Celestijnenlaan 200F, 3001 Leuven, Belgium

*E-mail: Daniel.Escudero@kuleuven.be

CONTENTS

1. Computational Methods and Theoretical Background for Rate Constants Calculations

PLQY and Lifetimes Predictions. We developed KinLuv, a Python-based kinetic simulation tool designed to predict prompt and delayed fluorescence lifetimes as well as PLQY using fully calculated *ab initio* rate constants as input. KinLuv is suited to modeling intricate multistate photophysical processes including fluorescence, phosphorescence, (reverse) internal conversion (IC), (r)ISC by solving coupled systems of ordinary differential equations (ODEs). The simulation framework consists of three main steps: excitation, decay, and PLQY evaluation. Required inputs include necessary rate constants and initial conditions, such as the number of absorbed photons (e.g., 1) and the excitation pulse width (e.g., 10 ps). For two- and three-state models, KinLuv provides analytical solutions, while for more sophisticated four- and five-state systems, it employs numerical simulations with separate timescales for excitation (e.g., 1 ns) and decay (e.g., 1 ms) to ensure accurate and stable results. By comprehensively accounting for all relevant transitions, KinLuv facilitates direct comparison with experimental data and provides clear insights into the underlying excited-state decay mechanisms. The accuracy of the simulated photophysical properties is inherently limited by uncertainties in the computed rate constants, which may arise from methodological approximations (e.g., validity of the harmonic oscillator approximation). These limitations are well described for the state-of-the art excited state decay rate constant theories[1] and they are further elaborated for the specific cases studied here in the Section 2.5. of manuscript.

Geometry Optimizations. The geometries of ground, singlet and triplet excited states were optimized using density functional theory (DFT)[2,3], time-dependent DFT (TD-DFT)[4,5], and Tamm-Dancoff approximation DFT (TDA-DFT)[6], respectively. The CAM-B3LYP functional[7] along with the 6-311G(d,p) basis set were employed for the TADF emitters DOBNA, DiKTa, and DQAO. The 6-31G(d,p) basis set was applied for the larger TADF molecule DABNA-1 and non-TADF systems DBT and PPDs-1, which is sufficiently accurate for the electronic states considered within the scope of this study. This computational protocol was applied to all subsequent electronic structure calculations, except for the adiabatic energy gap calculations. Grimme's D3 dispersion correction[8] was included for all the investigated molecules. Solvent effects were described using the solvation model based on density (SMD)[9] with toluene for DiKTa, cyclohexane for DBT, and dichloromethane for PPDs-1, to mimic the corresponding experimental conditions. All optimizations were performed using Gaussian (16A03) with default convergence criteria and grids[10], followed by frequency calculations to obtain the Hessian matrix and to confirm the absence of imaginary frequencies.

Adiabatic Energy Gap Calculations. The protocol described above was refined to improve the accuracy of the computed adiabatic energy gaps. Towards this end, single-point energy calculations on the respective optimized geometries were carried out with the spin-component-scaled (SCS)[11] second-order algebraic diagrammatic construction (ADC(2)) method[12] and the def2-TZVP basis set[13]. This level of theory has been proven highly accurate for the adiabatic energy gap of the first singlet and triplet excited states of organic emitters, including e.g., MR-TADF dyes[14–16]. The resolution of identity (RI) approximation was employed with no frozen core approximation[17]. These calculations were performed with the Turbomole (7.7)[18].

Excited State Decay Rate Constants. Transition dipole moments (TDMs) were computed using TD(A)-CAM-B3LYP at the S_1 and S_0 optimized geometries. Nonadiabatic coupling matrix elements (NACMEs) were determined at TD-CAM-B3LYP level of theory and evaluated at the optimized geometries of corresponding electronic states, typically those of the final states, using the electron-translation factors (ETF) correction, as implemented in Q-CHEM (5.3)[19]. Spin orbit coupling matrix elements (SOCMEs) were evaluated at the TDA-CAM-B3LYP level of theory with ORCA (5.0.4, 6.0)[20,21], specifying a higher grid (defgrid3) and four-center integrals for both Coulomb and exchange terms (SOCFlags = 1,4,4,1). Excited-state decay rate constants were computed using the thermal vibration-correlation function (TVCF) formalism[22], also known as the time-dependent approach. The adiabatic Hessian (AH) vibronic model[23] was chosen, which incorporates Duschinsky rotation effects. We employed the previously optimized geometries, gradients, Hessian matrices, TDMs, NACMEs, and SOCMEs, together with adiabatic energy gaps obtained from SCS-ADC(2). Calculations were carried out at room temperature (~300 K) in the vibronic framework, and a Lorentzian broadening with a half width at half maximum (HWHM) of 10 cm^{-1} was applied. Fluorescence and IC rate constants were evaluated with FCClasses (3.0.1)[24], while phosphorescence and (r)ISC rates were computed using ORCA (5.0.4, 6.0). HT vibronic coupling was included in the radiative and ISC calculations, whereas IC rate constants can only be treated under the Franck-Condon (FC) approximation.

Fermi's Golden Rule (FGR). The transition rate constant (k_{if}) between the initial state and the final state is given by FGR[25]:

$$k_{if} = \frac{2\pi}{\hbar} \left|\left\langle \Psi_f \middle| \widehat{\mathcal{H}} \middle| \Psi_i \right\rangle\right|^2 \rho \tag{S1.1}$$

where Ψ_i and Ψ_f are the total wave functions (electronic and vibrational) of the initial and final states, ρ is the density of states and $\left|\left\langle \Psi_f \middle| \widehat{\mathcal{H}} \middle| \Psi_i \right\rangle\right|$ is the matrix element of perturbation $\widehat{\mathcal{H}}$ between the initial and final states. Moreover, the total wave function (Ψ) can be approximated by the product of its electronic (Φ) and vibrational parts (Θ) following the Born-Oppenheimer (BO) approximation[26]. By further applying the Condon approximation[27], eq S1.1 can be rewritten as:

$$k_{if} = \frac{2\pi}{\hbar} \sum_{\nu_i,\nu_f} P_{i,\nu_i}(T) \left|\left\langle \Theta_{f,\nu_f} \middle| \left\langle \Phi_f \middle| \widehat{\mathcal{H}} \middle| \Phi_i \right\rangle \middle| \Theta_{i,\nu_i} \right\rangle\right|^2 \delta\left(E_{f,\nu_f} - E_{i,\nu_i}\right) \tag{S1.2}$$

where the summation is carried out over all vibrational states (ν_i, ν_f) of the initial (i, ν_i) and final ($f,\ \nu_f$) electronic states, $P_{i,\nu_i}(T)$ is the Boltzmann population of the initial vibrational level at a temperature T, $\hbar$ is the reduced Planck's constant, and δ is the Dirac delta function which selects the energy corresponding to the transition. The three classes of rate constants are computed via FGR with different perturbing operators[28,29]: the radiative rate constant k_{r} is obtained by using the electric dipole (ELD) operator as the perturbation matrix; the rate constant of intersystem crossing (ISC) k_{ISC} is calculated by employing the spin orbit coupling (SOC) operator; the rate constant of internal conversion (IC) k_{IC} is derived with the nonadiabatic coupling (NAC) operator. An essential component of all rate constant calculations is the overlap between vibrational wave functions of the two electronic states involved, which are typically evaluated with a harmonic oscillator approximation. Adiabatic Hessian (AH) is one of the popular vibronic models,

where each state's vibrational wave functions are evaluated at its own optimized geometry (the Hessian at its minimum)[30]. Vibrational modes are then mapped onto one another via the Duschinsky rotation[31]. AH can break down if the two states' geometries differ excessively.

Radiative Rate Constants. When the perturbation ($\widehat{\mathcal{H}}$) is replaced by the ELD ($\hat{\mu}$), the radiative rate constant can be obtained with eq S1.2. The transition dipole moments (TDMs) $\vec{\mu}_{if}$ depending on the vibrational normal coordinate (Q) can be expanded as:

$$\vec{\mu}_{if}(Q) = \left(\langle \Phi_f | \hat{\mu} | \Phi_i \rangle\right)_0 + \sum_k \left(\frac{\partial \langle \Phi_f | \hat{\mu} | \Phi_i \rangle}{\partial Q_k}\right)_0 Q_k \tag{S1.3}$$

where $\left(\langle \Phi_f | \hat{\mu} | \Phi_i \rangle\right)_0$ is the zeroth-order TMD in the Franck-Condon (FC) approximation, and the second term refers to the so-called Herzberg-Teller (HT) effects[32], which arises from the first-order dependence of the TDMs on the nuclear displacements. The summation runs over all normal vibrational modes (Q_k).

ISC Rate Constants. When the perturbation ($\widehat{\mathcal{H}}$) becomes the SOC operator ($\widehat{\mathcal{H}}_{\mathrm{SOC}}$), the ISC rate constant can be obtained with eq S1.2. Analogously to that for radiative rate constants, an HT-like expression for ISC also exists. The spin orbit coupling matrix elements (SOCMEs) include not only the zeroth-order term $\left(\langle \Phi_f | \widehat{\mathcal{H}}_{\mathrm{SOC}} | \Phi_i \rangle\right)_0$ but also the first-order expansion with respect to the normal coordinates (Q), which accounts for the vibronic spin-orbit interactions[33]:

$$SOC(Q) = \left(\langle \Phi_f | \widehat{\mathcal{H}}_{\mathrm{SOC}} | \Phi_i \rangle\right)_0 + \sum_k \left(\frac{\partial \langle \Phi_f | \widehat{\mathcal{H}}_{\mathrm{SOC}} | \Phi_i \rangle}{\partial Q_k}\right)_0 Q_k \tag{S1.4}$$

IC Rate Constants. The IC rate constant, expressed in terms of NAC operator, can be obtained as follows[34]:

$$k_{\mathrm{IC}} = \sum_{k,l} \frac{R_{kl}}{\hbar^2} \int_{-\infty}^{\infty} e^{i\omega_{if}t} Z_{iv}^{-1} \rho_{\mathrm{IC},kl}(t,T)\, dt \tag{S1.5}$$

where $\rho_{\mathrm{IC},kl}(t,T)$ denotes the thermal vibration correlation function (TVCF) for IC, Z_{iv} is the partition function, and R_{kl} is the electronic coupling part of the NAC. Similar to TDMs, nonadiabatic coupling matrix elements (NACMEs) can be obtained from quantum chemical calculations. However, HT-like expansion for the IC rate constant is not yet widely implemented in the available codes.

2. Ordinary Differential Equations (ODEs) for Different Models of the Excitation Period

Two-state Model (S_0, S_1):

$$-[S_0]k_{ABS}^{S0\to S1} + [S_1]\left(k_{FL}^{S1\to S0} + k_{IC}^{S1\to S0}\right) = \frac{d[S_0]}{dt} \tag{S2.1}$$

$$[S_0]k_{ABS}^{S0\to S1} - [S_1]\left(k_{FL}^{S1\to S0} + k_{IC}^{S1\to S0}\right) = \frac{d[S_1]}{dt} \tag{S2.2}$$

Three-state Model (S_0, S_1, T_1):

$$-[S_0]k_{ABS}^{S0\to S1} + [S_1]\left(k_{FL}^{S1\to S0} + k_{IC}^{S1\to S0}\right) + [T_1]\left(k_{PH}^{T1\to S0} + k_{ISC}^{T1\to S0}\right) = \frac{d[S_0]}{dt} \tag{S2.3}$$

$$[S_0]k_{ABS}^{S0\to S1} - [S_1]\left(k_{ISC}^{S1\to T1} + k_{FL}^{S1\to S0} + k_{IC}^{S1\to S0}\right) + [T_1]k_{rISC}^{T1\to S1} = \frac{d[S_1]}{dt} \tag{S2.4}$$

$$[S_1]k_{ISC}^{S1\to T1} - [T_1]\left(k_{PH}^{T1\to S0} + k_{ISC}^{T1\to S0} + k_{rISC}^{T1\to S1}\right) = \frac{d[T_1]}{dt} \tag{S2.5}$$

Four-state Model (S_0, S_1, T_1, T_2):

$$-[S_0]k_{ABS}^{S0\to S1} + [S_1]\left(k_{FL}^{S1\to S0} + k_{IC}^{S1\to S0}\right) + [T_1]\left(k_{PH}^{T1\to S0} + k_{ISC}^{T1\to S0}\right) = \frac{d[S_0]}{dt} \tag{S2.6}$$

$$[S_0]k_{ABS}^{S0\to S1} - [S_1]\left(k_{ISC}^{S1\to T1} + k_{ISC}^{S1\to T2} + k_{FL}^{S1\to S0} + k_{IC}^{S1\to S0}\right) + [T_1]k_{rISC}^{T1\to S1} + [T_2]k_{rISC}^{T2\to S1} = \frac{d[S_1]}{dt} \tag{S2.7}$$

$$[S_1]k_{ISC}^{S1\to T1} - [T_1]\left(k_{PH}^{T1\to S0} + k_{ISC}^{T1\to S0} + k_{rISC}^{T1\to S1} + k_{rIC}^{T1\to T2}\right) + [T_2]k_{IC}^{T2\to T1} = \frac{d[T_1]}{dt} \tag{S2.8}$$

$$[S_1]k_{ISC}^{S1\to T2} + [T_1]k_{rIC}^{T1\to T2} - [T_2]\left(k_{rISC}^{T2\to S1} + k_{IC}^{T2\to T1}\right) = \frac{d[T_2]}{dt} \tag{S2.9}$$

Five-state Model (S_0, S_1, S_2, T_1, T_2):

$$-[S_0]k_{ABS}^{S0\to S2} + [S_1]\left(k_{FL}^{S1\to S0} + k_{IC}^{S1\to S0}\right) + [S_2]\left(k_{FL}^{S2\to S0} + k_{IC}^{S2\to S0}\right) + [T_1]\left(k_{PH}^{T1\to S0} + k_{ISC}^{T1\to S0}\right) = \frac{d[S_0]}{dt} \tag{S2.10}$$

$$-[S_1]\left(k_{ISC}^{S1\to T1} + k_{ISC}^{S1\to T2} + k_{FL}^{S1\to S0} + k_{IC}^{S1\to S0} + k_{rIC}^{S1\to S2}\right) + [S_2]k_{IC}^{S2\to S1} + [T_1]k_{rISC}^{T1\to S1} + [T_2]k_{rISC}^{T2\to S1} = \frac{d[S_1]}{dt} \tag{S2.11}$$

$$[S_0]k_{ABS}^{S0\to S2} + [S_1]k_{rIC}^{S1\to S2} - [S_2]\left(k_{IC}^{S2\to S1} + k_{ISC}^{S2\to T1} + k_{ISC}^{S2\to T2} + k_{FL}^{S2\to S0} + k_{IC}^{S2\to S0}\right) + [T_1]k_{rISC}^{T1\to S2} + [T_2]k_{rISC}^{T2\to S2} = \frac{d[S_2]}{dt} \tag{S2.12}$$

$$[S_1]k_{ISC}^{S1\to T1} + [S_2]k_{ISC}^{S2\to T1} - [T_1]\left(k_{PH}^{T1\to S0} + k_{ISC}^{T1\to S0} + k_{rISC}^{T1\to S1} + k_{rISC}^{T1\to S2} + k_{rIC}^{T1\to T2}\right) + [T_2]k_{IC}^{T2\to T1} = \frac{d[T_1]}{dt} \tag{S2.13}$$

$$[S_1]k_{ISC}^{S1\to T2} + [S_2]k_{ISC}^{S2\to T2} + [T_1]k_{rIC}^{T1\to T2} - [T_2]\left(k_{rISC}^{T2\to S1} + k_{rISC}^{T2\to S2} + k_{IC}^{T2\to T1}\right) = \frac{d[T_2]}{dt} \tag{S2.14}$$

The transient photoluminescence decay curve is typically measured following a short excitation pulse. Equations (eq S2.1-S2.14) above describe the excited-state population kinetics during this excitation period. Consequently, the excited-state populations at the end of the excitation pulse serve as the initial conditions for the subsequent decay period. To solve the ODEs, the absorption rate ($k_{ABS}^{S0\to S1}$, $k_{ABS}^{S0\to S2}$) and the duration of the excitation pulse t_{pulse} must be specified. These parameters will not affect the prompt or delayed fluorescence lifetimes during the decay period. In this case study, $k_{ABS}^{S0\to S1} = 1 \times 10^{13}\ (s^{-1})$, $k_{ABS}^{S0\to S2} = 1 \times 10^{13}\ (s^{-1})$, $t_{pulse} = 10\ (ps)$.

3. ODEs in Vector-Matrix Form for Different Models of the Decay Period ($k_{ABS}^{S0\to S1}=0$, $k_{ABS}^{S0\to S2}=0$)

Two-state Model (S_0, S_1):

$$\frac{\mathrm{d}}{\mathrm{d}t}\begin{pmatrix}[S_0]\\[S_1]\end{pmatrix}=\begin{pmatrix}0 & \left(k_{FL}^{S1\to S0}+k_{IC}^{S1\to S0}\right)\\ 0 & -\left(k_{FL}^{S1\to S0}+k_{IC}^{S1\to S0}\right)\end{pmatrix}\begin{pmatrix}[S_0]\\[S_1]\end{pmatrix} \tag{S3.1}$$

Three-state Model (S_0, S_1, T_1):

$$\frac{\mathrm{d}}{\mathrm{d}t}\begin{pmatrix}[S_0]\\[S_1]\\[T_1]\end{pmatrix}=\begin{pmatrix}0 & \left(k_{FL}^{S1\to S0}+k_{IC}^{S1\to S0}\right) & \left(k_{PH}^{T1\to S0}+k_{ISC}^{T1\to S0}\right)\\ 0 & -\left(k_{ISC}^{S1\to T1}+k_{FL}^{S1\to S0}+k_{IC}^{S1\to S0}\right) & k_{rISC}^{T1\to S1}\\ 0 & k_{ISC}^{S1\to T1} & -\left(k_{PH}^{T1\to S0}+k_{ISC}^{T1\to S0}+k_{rISC}^{T1\to S1}\right)\end{pmatrix}\begin{pmatrix}[S_0]\\[S_1]\\[T_1]\end{pmatrix} \tag{S3.2}$$

Four-state Model (S_0, S_1, T_1, T_2):

$$\frac{\mathrm{d}}{\mathrm{d}t}\begin{pmatrix}[S_0]\\[S_1]\\[T_1]\\[T_2]\end{pmatrix}=\begin{pmatrix}0 & \left(k_{FL}^{S1\to S0}+k_{IC}^{S1\to S0}\right) & \left(k_{PH}^{T1\to S0}+k_{ISC}^{T1\to S0}\right) & 0\\ 0 & -\left(k_{ISC}^{S1\to T1}+k_{ISC}^{S1\to T2}+k_{FL}^{S1\to S0}+k_{IC}^{S1\to S0}\right) & k_{rISC}^{T1\to S1} & k_{rISC}^{T2\to S1}\\ 0 & k_{ISC}^{S1\to T1} & -\left(k_{PH}^{T1\to S0}+k_{ISC}^{T1\to S0}+k_{rISC}^{T1\to S1}+k_{rIC}^{T1\to T2}\right) & k_{IC}^{T2\to T1}\\ 0 & k_{ISC}^{S1\to T2} & k_{rIC}^{T1\to T2} & -\left(k_{rISC}^{T2\to S1}+k_{IC}^{T2\to T1}\right)\end{pmatrix}\begin{pmatrix}[S_0]\\[S_1]\\[T_1]\\[T_2]\end{pmatrix} \tag{S3.3}$$

Five-state Model (S_0, S_1, S_2, T_1, T_2):

$$\frac{\mathrm{d}}{\mathrm{d}t}\begin{pmatrix}[S_0]\\[S_1]\\[S_2]\\[T_1]\\[T_2]\end{pmatrix}=K\begin{pmatrix}[S_0]\\[S_1]\\[S_2]\\[T_1]\\[T_2]\end{pmatrix} \tag{S3.4}$$

$$K=\begin{pmatrix}0 & \left(k_{FL}^{S1\to S0}+k_{IC}^{S1\to S0}\right) & \left(k_{FL}^{S2\to S0}+k_{IC}^{S2\to S0}\right) & \left(k_{PH}^{T1\to S0}+k_{ISC}^{T1\to S0}\right) & 0\\ 0 & \sum S_1 & k_{IC}^{S2\to S1} & k_{rISC}^{T1\to S1} & k_{rISC}^{T2\to S1}\\ 0 & k_{rIC}^{S1\to S2} & \sum S_2 & k_{rISC}^{T1\to S2} & k_{rISC}^{T2\to S2}\\ 0 & k_{ISC}^{S1\to T1} & k_{ISC}^{S2\to T1} & \sum T_1 & k_{IC}^{T2\to T1}\\ 0 & k_{ISC}^{S1\to T2} & k_{ISC}^{S2\to T2} & k_{rIC}^{T1\to T2} & \sum T_2\end{pmatrix} \tag{S3.5}$$

$$\sum S_1=-\left(k_{ISC}^{S1\to T1}+k_{ISC}^{S1\to T2}+k_{FL}^{S1\to S0}+k_{IC}^{S1\to S0}+k_{rIC}^{S1\to S2}\right) \tag{S3.6}$$

$$\sum S_2=-\left(k_{IC}^{S2\to S1}+k_{ISC}^{S2\to T1}+k_{ISC}^{S2\to T2}+k_{FL}^{S2\to S0}+k_{IC}^{S2\to S0}\right) \tag{S3.7}$$

$$\sum T_1=-\left(k_{PH}^{T1\to S0}+k_{ISC}^{T1\to S0}+k_{rISC}^{T1\to S1}+k_{rISC}^{T1\to S2}+k_{rIC}^{T1\to T2}\right) \tag{S3.8}$$

$$\sum T_2=-\left(k_{rISC}^{T2\to S1}+k_{rISC}^{T2\to S2}+k_{IC}^{T2\to T1}\right) \tag{S3.9}$$

The general solution of ODEs is given by

$$\vec{N}(t)=\sum_{i=1}^{n}c_i\vec{v_i}e^{\lambda_i t} \tag{S3.10}$$

where $\vec{N}(t)$ is the state population vector, $\vec{v_i}$ denotes the eigenvector, λ_i is the corresponding eigenvalue and c_i is the coefficient associated with the matrix. For example, in the case of the three-state model (S_0, S_1, T_1), These parameters can be determined

$$\begin{pmatrix}\lambda_1\\ \lambda_2\\ \lambda_3\end{pmatrix}=\begin{pmatrix}0\\ -1/2\left(k_{sum}^{S1}-k_{sum}^{T1}+\sqrt{(k_{sum}^{S1}-k_{sum}^{T1})^2+4k_{ISC}^{S1\to T1}k_{rISC}^{T1\to S1}}\right)\\ -1/2\left(k_{sum}^{S1}-k_{sum}^{T1}-\sqrt{(k_{sum}^{S1}-k_{sum}^{T1})^2+4k_{ISC}^{S1\to T1}k_{rISC}^{T1\to S1}}\right)\end{pmatrix} \tag{S3.11}$$

$$\vec{v_1}=\begin{pmatrix}1\\0\\0\end{pmatrix},\vec{v_2}=\begin{pmatrix}-\left(\lambda_2+k_{sum}^{S1}+k_{rISC}^{T1\to S1}\right)\\ k_{rISC}^{T1\to S1}\\ \lambda_2+k_{sum}^{S1}\end{pmatrix},\vec{v_3}=\begin{pmatrix}-\left(\lambda_3+k_{sum}^{S1}+k_{rISC}^{T1\to S1}\right)\\ k_{rISC}^{T1\to S1}\\ \lambda_3+k_{sum}^{S1}\end{pmatrix} \tag{S3.12}$$

where $k_{sum}^{S1}=k_{ISC}^{S1\to T1}+k_{FL}^{S1\to S0}+k_{IC}^{S1\to S0}$, $k_{sum}^{T1}=k_{PH}^{T1\to S0}+k_{ISC}^{T1\to S0}+k_{rISC}^{T1\to S1}$. Consequently, the excited state populations can be described as follows:

$$\begin{pmatrix}[S_0]\\[S_1]\\[T_1]\end{pmatrix}=\begin{pmatrix}c_1-c_2\left(k_{sum}^{S1}+k_{rISC}^{T1\to S1}-k_{PF}\right)e^{-k_{PF}t}-c_3\left(k_{sum}^{S1}+k_{rISC}^{T1\to S1}-k_{DF}\right)e^{-k_{DF}t}\\ c_2k_{rISC}^{T1\to S1}e^{-k_{PF}t}+c_3k_{rISC}^{T1\to S1}e^{-k_{DF}t}\\ c_2(k_{sum}^{S1}-k_{PF})e^{-k_{PF}t}+c_3(k_{sum}^{S1}-k_{DF})e^{-k_{DF}t}\end{pmatrix} \tag{S3.13}$$

where $k_{PF}=-\lambda_2$, $k_{DF}=-\lambda_3$, and coefficients c_i can be obtained from eq S3.14.

$$\begin{pmatrix} 1 & -\left(\lambda_2 + k_{\mathrm{sum}}^{\mathrm{S1}} + k_{\mathrm{rISC}}^{\mathrm{T1}\to\mathrm{S1}}\right) & -\left(\lambda_3 + k_{\mathrm{sum}}^{\mathrm{S1}} + k_{\mathrm{rISC}}^{\mathrm{T1}\to\mathrm{S1}}\right) \\ 0 & k_{\mathrm{rISC}}^{\mathrm{T1}\to\mathrm{S1}} & k_{\mathrm{rISC}}^{\mathrm{T1}\to\mathrm{S1}} \\ 0 & \lambda_2 + k_{\mathrm{sum}}^{\mathrm{S1}} & \lambda_3 + k_{\mathrm{sum}}^{\mathrm{S1}} \end{pmatrix} \begin{pmatrix} c_1 \\ c_2 \\ c_3 \end{pmatrix} = \begin{pmatrix} [\mathrm{S}_0]_{t=0} \\ [\mathrm{S}_1]_{t=0} \\ [\mathrm{T}_1]_{t=0} \end{pmatrix} \tag{S3.14}$$

$$\begin{pmatrix} c_1 \\ c_2 \\ c_3 \end{pmatrix} = \begin{pmatrix} [\mathrm{S}_0]_{t=0} + [\mathrm{S}_1]_{t=0} + [\mathrm{T}_1]_{t=0} \\ \dfrac{(k_{\mathrm{sum}}^{\mathrm{S1}} - k_{\mathrm{DF}})[\mathrm{S}_1]_{t=0} - k_{\mathrm{rISC}}^{\mathrm{T1}\to\mathrm{S1}}[\mathrm{T}_1]_{t=0}}{k_{\mathrm{rISC}}^{\mathrm{T1}\to\mathrm{S1}}(k_{\mathrm{PF}} - k_{\mathrm{DF}})} \\ \dfrac{-(k_{\mathrm{sum}}^{\mathrm{S1}} - k_{\mathrm{PF}})[\mathrm{S}_1]_{t=0} + k_{\mathrm{rISC}}^{\mathrm{T1}\to\mathrm{S1}}[\mathrm{T}_1]_{t=0}}{k_{\mathrm{rISC}}^{\mathrm{T1}\to\mathrm{S1}}(k_{\mathrm{PF}} - k_{\mathrm{DF}})} \end{pmatrix} \tag{S3.15}$$

Especially when $[\mathrm{S}_0]_{t=0} = [\mathrm{T}_1]_{t=0} = 0$, $[\mathrm{S}_1]$ and $[\mathrm{T}_1]$ can be written as below:

$$[\mathrm{S}_1] = \frac{[\mathrm{S}_1]_{t=0}}{(k_{\mathrm{PF}} - k_{\mathrm{DF}})}(k_{\mathrm{sum}}^{\mathrm{S1}} - k_{\mathrm{DF}})e^{-k_{\mathrm{PF}}t} + \frac{[\mathrm{S}_1]_{t=0}}{(k_{\mathrm{PF}} - k_{\mathrm{DF}})}e^{-k_{\mathrm{DF}}t} \tag{S3.16}$$

$$[\mathrm{T}_1] = \frac{[\mathrm{S}_1]_{t=0}k_{\mathrm{ISC}}^{\mathrm{S1}\to\mathrm{T1}}}{(k_{\mathrm{PF}} - k_{\mathrm{DF}})} - e^{-k_{\mathrm{PF}}t} + \frac{[\mathrm{S}_1]_{t=0}k_{\mathrm{ISC}}^{\mathrm{S1}\to\mathrm{T1}}}{(k_{\mathrm{PF}} - k_{\mathrm{DF}})}e^{-k_{\mathrm{DF}}t} \tag{S3.17}$$

4. Ordinary Algebraic Equations for Different Models Under Steady State Approximation (SSA)

Two-state Model (S_0, S_1):

$$\begin{pmatrix} -k_{\mathrm{ABS}}^{\mathrm{S0}\to\mathrm{S1}} & \left(k_{\mathrm{FL}}^{\mathrm{S1}\to\mathrm{S0}}+k_{\mathrm{IC}}^{\mathrm{S1}\to\mathrm{S0}}\right) \\ k_{\mathrm{ABS}}^{\mathrm{S0}\to\mathrm{S1}} & -\left(k_{\mathrm{FL}}^{\mathrm{S1}\to\mathrm{S0}}+k_{\mathrm{IC}}^{\mathrm{S1}\to\mathrm{S0}}\right) \end{pmatrix}\begin{pmatrix}[\mathrm{S_0}]\\[\mathrm{S_1}]\end{pmatrix}=0 \tag{S4.1}$$

Three-state Model (S_0, S_1, T_1):

$$\begin{pmatrix} -k_{\mathrm{ABS}}^{\mathrm{S0}\to\mathrm{S1}} & \left(k_{\mathrm{FL}}^{\mathrm{S1}\to\mathrm{S0}}+k_{\mathrm{IC}}^{\mathrm{S1}\to\mathrm{S0}}\right) & \left(k_{\mathrm{PH}}^{\mathrm{T1}\to\mathrm{S0}}+k_{\mathrm{ISC}}^{\mathrm{T1}\to\mathrm{S0}}\right) \\ k_{\mathrm{ABS}}^{\mathrm{S0}\to\mathrm{S1}} & -\left(k_{\mathrm{ISC}}^{\mathrm{S1}\to\mathrm{T1}}+k_{\mathrm{FL}}^{\mathrm{S1}\to\mathrm{S0}}+k_{\mathrm{IC}}^{\mathrm{S1}\to\mathrm{S0}}\right) & k_{\mathrm{rISC}}^{\mathrm{T1}\to\mathrm{S1}} \\ 0 & k_{\mathrm{ISC}}^{\mathrm{S1}\to\mathrm{T1}} & -\left(k_{\mathrm{PH}}^{\mathrm{T1}\to\mathrm{S0}}+k_{\mathrm{ISC}}^{\mathrm{T1}\to\mathrm{S0}}+k_{\mathrm{rISC}}^{\mathrm{T1}\to\mathrm{S1}}\right) \end{pmatrix}\begin{pmatrix}[\mathrm{S_0}]\\[\mathrm{S_1}]\\[\mathrm{T_1}]\end{pmatrix}=0 \tag{S4.2}$$

Four-state Model (S_0, S_1, T_1, T_2):

$$\begin{pmatrix} -k_{\mathrm{ABS}}^{\mathrm{S0}\to\mathrm{S1}} & \left(k_{\mathrm{FL}}^{\mathrm{S1}\to\mathrm{S0}}+k_{\mathrm{IC}}^{\mathrm{S1}\to\mathrm{S0}}\right) & \left(k_{\mathrm{PH}}^{\mathrm{T1}\to\mathrm{S0}}+k_{\mathrm{ISC}}^{\mathrm{T1}\to\mathrm{S0}}\right) & 0 \\ k_{\mathrm{ABS}}^{\mathrm{S0}\to\mathrm{S1}} & -\left(k_{\mathrm{ISC}}^{\mathrm{S1}\to\mathrm{T1}}+k_{\mathrm{ISC}}^{\mathrm{S1}\to\mathrm{T2}}+k_{\mathrm{FL}}^{\mathrm{S1}\to\mathrm{S0}}+k_{\mathrm{IC}}^{\mathrm{S1}\to\mathrm{S0}}\right) & k_{\mathrm{rISC}}^{\mathrm{T1}\to\mathrm{S1}} & k_{\mathrm{rISC}}^{\mathrm{T2}\to\mathrm{S1}} \\ 0 & k_{\mathrm{ISC}}^{\mathrm{S1}\to\mathrm{T1}} & -\left(k_{\mathrm{PH}}^{\mathrm{T1}\to\mathrm{S0}}+k_{\mathrm{ISC}}^{\mathrm{T1}\to\mathrm{S0}}+k_{\mathrm{rISC}}^{\mathrm{T1}\to\mathrm{S1}}+k_{\mathrm{rIC}}^{\mathrm{T1}\to\mathrm{T2}}\right) & k_{\mathrm{IC}}^{\mathrm{T2}\to\mathrm{T1}} \\ 0 & k_{\mathrm{ISC}}^{\mathrm{S1}\to\mathrm{T2}} & k_{\mathrm{rIC}}^{\mathrm{T1}\to\mathrm{T2}} & -\left(k_{\mathrm{rISC}}^{\mathrm{T2}\to\mathrm{S1}}+k_{\mathrm{IC}}^{\mathrm{T2}\to\mathrm{T1}}\right) \end{pmatrix}\begin{pmatrix}[\mathrm{S_0}]\\[\mathrm{S_1}]\\[\mathrm{T_1}]\\[\mathrm{T_2}]\end{pmatrix}=0 \tag{S4.3}$$

Five-state Model (S_0, S_1, S_2, T_1, T_2):

$$K\begin{pmatrix}[\mathrm{S_0}]\\[\mathrm{S_1}]\\[\mathrm{S_2}]\\[\mathrm{T_1}]\\[\mathrm{T_2}]\end{pmatrix}=0 \tag{S4.4}$$

$$K=\begin{pmatrix} -k_{\mathrm{ABS}}^{\mathrm{S0}\to\mathrm{S2}} & \left(k_{\mathrm{FL}}^{\mathrm{S1}\to\mathrm{S0}}+k_{\mathrm{IC}}^{\mathrm{S1}\to\mathrm{S0}}\right) & \left(k_{\mathrm{FL}}^{\mathrm{S2}\to\mathrm{S0}}+k_{\mathrm{IC}}^{\mathrm{S2}\to\mathrm{S0}}\right) & \left(k_{\mathrm{PH}}^{\mathrm{T1}\to\mathrm{S0}}+k_{\mathrm{ISC}}^{\mathrm{T1}\to\mathrm{S0}}\right) & 0 \\ 0 & \sum \mathrm{S_1} & k_{\mathrm{IC}}^{\mathrm{S2}\to\mathrm{S1}} & k_{\mathrm{rISC}}^{\mathrm{T1}\to\mathrm{S1}} & k_{\mathrm{rISC}}^{\mathrm{T2}\to\mathrm{S1}} \\ k_{\mathrm{ABS}}^{\mathrm{S0}\to\mathrm{S2}} & k_{\mathrm{rIC}}^{\mathrm{S1}\to\mathrm{S2}} & \sum \mathrm{S_2} & k_{\mathrm{rISC}}^{\mathrm{T1}\to\mathrm{S2}} & k_{\mathrm{rISC}}^{\mathrm{T2}\to\mathrm{S2}} \\ 0 & k_{\mathrm{ISC}}^{\mathrm{S1}\to\mathrm{T1}} & k_{\mathrm{ISC}}^{\mathrm{S2}\to\mathrm{T1}} & \sum \mathrm{T_1} & k_{\mathrm{IC}}^{\mathrm{T2}\to\mathrm{T1}} \\ 0 & k_{\mathrm{ISC}}^{\mathrm{S1}\to\mathrm{T2}} & k_{\mathrm{ISC}}^{\mathrm{S2}\to\mathrm{T2}} & k_{\mathrm{rIC}}^{\mathrm{T1}\to\mathrm{T2}} & \sum \mathrm{T_2} \end{pmatrix} \tag{S4.5}$$

$$\sum \mathrm{S_1}=-\left(k_{\mathrm{ISC}}^{\mathrm{S1}\to\mathrm{T1}}+k_{\mathrm{ISC}}^{\mathrm{S1}\to\mathrm{T2}}+k_{\mathrm{FL}}^{\mathrm{S1}\to\mathrm{S0}}+k_{\mathrm{IC}}^{\mathrm{S1}\to\mathrm{S0}}+k_{\mathrm{rIC}}^{\mathrm{S1}\to\mathrm{S2}}\right) \tag{S4.6}$$

$$\sum \mathrm{S_2}=-\left(k_{\mathrm{IC}}^{\mathrm{S2}\to\mathrm{S1}}+k_{\mathrm{ISC}}^{\mathrm{S2}\to\mathrm{T1}}+k_{\mathrm{ISC}}^{\mathrm{S2}\to\mathrm{T2}}+k_{\mathrm{FL}}^{\mathrm{S2}\to\mathrm{S0}}+k_{\mathrm{IC}}^{\mathrm{S2}\to\mathrm{S0}}\right) \tag{S4.7}$$

$$\sum \mathrm{T_1}=-\left(k_{\mathrm{PH}}^{\mathrm{T1}\to\mathrm{S0}}+k_{\mathrm{ISC}}^{\mathrm{T1}\to\mathrm{S0}}+k_{\mathrm{rISC}}^{\mathrm{T1}\to\mathrm{S1}}+k_{\mathrm{rISC}}^{\mathrm{T1}\to\mathrm{S2}}+k_{\mathrm{rIC}}^{\mathrm{T1}\to\mathrm{T2}}\right) \tag{S4.8}$$

$$\sum \mathrm{T_2}=-\left(k_{\mathrm{rISC}}^{\mathrm{T2}\to\mathrm{S1}}+k_{\mathrm{rISC}}^{\mathrm{T2}\to\mathrm{S2}}+k_{\mathrm{IC}}^{\mathrm{T2}\to\mathrm{T1}}\right) \tag{S4.9}$$

The quantum yield (Φ_i) of a photophysical process is defined as

$$\Phi_i=\frac{\text{Number of molecules undergoing that process}}{\text{Number of photons absorbed by the reactant}} \tag{S4.10}$$

The two-state model under SSA (eq S4.1) yields the following relationship:

$$[\mathrm{S_0}]k_{\mathrm{ABS}}^{\mathrm{S0}\to\mathrm{S1}}=[\mathrm{S_1}]\left(k_{\mathrm{FL}}^{\mathrm{S1}\to\mathrm{S0}}+k_{\mathrm{IC}}^{\mathrm{S1}\to\mathrm{S0}}\right) \tag{S4.11}$$

where $[\mathrm{S_0}]k_{\mathrm{ABS}}^{\mathrm{S0}\to\mathrm{S1}}$ denotes the number of molecules excited per unit volume per unit time, equals the number of photons absorbed per unit volume per unit time under the one-photon absorption mechanism.

Accordingly, the photoluminescence quantum yield (PLQY) of fluorescence is given by:

$$\Phi_{\mathrm{FL}}=\frac{[\mathrm{S_1}]k_{\mathrm{FL}}^{\mathrm{S1}\to\mathrm{S0}}}{[\mathrm{S_0}]k_{\mathrm{ABS}}^{\mathrm{S0}\to\mathrm{S1}}}=\frac{[\mathrm{S_1}]k_{\mathrm{FL}}^{\mathrm{S1}\to\mathrm{S0}}}{[\mathrm{S_1}](k_{\mathrm{FL}}^{\mathrm{S1}\to\mathrm{S0}}+k_{\mathrm{IC}}^{\mathrm{S1}\to\mathrm{S0}})}=\frac{k_{\mathrm{FL}}^{\mathrm{S1}\to\mathrm{S0}}}{(k_{\mathrm{FL}}^{\mathrm{S1}\to\mathrm{S0}}+k_{\mathrm{IC}}^{\mathrm{S1}\to\mathrm{S0}})} \tag{S4.12}$$

Similarly, the three-state model under SSA (eq S4.2) gives:

$$[\mathrm{S_0}]k_{\mathrm{ABS}}^{\mathrm{S0}\to\mathrm{S1}}=[\mathrm{S_1}]\left(k_{\mathrm{FL}}^{\mathrm{S1}\to\mathrm{S0}}+k_{\mathrm{IC}}^{\mathrm{S1}\to\mathrm{S0}}\right)+[\mathrm{T_1}]\left(k_{\mathrm{PH}}^{\mathrm{T1}\to\mathrm{S0}}+k_{\mathrm{ISC}}^{\mathrm{T1}\to\mathrm{S0}}\right) \tag{S4.13}$$

$$[\mathrm{T_1}]=[\mathrm{S_1}]\frac{k_{\mathrm{ISC}}^{\mathrm{S1}\to\mathrm{T1}}}{(k_{\mathrm{PH}}^{\mathrm{T1}\to\mathrm{S0}}+k_{\mathrm{ISC}}^{\mathrm{T1}\to\mathrm{S0}}+k_{\mathrm{rISC}}^{\mathrm{T1}\to\mathrm{S1}})} \tag{S4.14}$$

Therefore, PLQY of fluorescence for three-state model is given by:

$$\Phi_{\mathrm{FL}}=\frac{[\mathrm{S_1}]k_{\mathrm{FL}}^{\mathrm{S1}\to\mathrm{S0}}}{[\mathrm{S_0}]k_{\mathrm{ABS}}^{\mathrm{S0}\to\mathrm{S1}}}=\frac{[\mathrm{S_1}]k_{\mathrm{FL}}^{\mathrm{S1}\to\mathrm{S0}}}{[\mathrm{S_1}](k_{\mathrm{FL}}^{\mathrm{S1}\to\mathrm{S0}}+k_{\mathrm{IC}}^{\mathrm{S1}\to\mathrm{S0}})+[\mathrm{T_1}](k_{\mathrm{PH}}^{\mathrm{T1}\to\mathrm{S0}}+k_{\mathrm{ISC}}^{\mathrm{T1}\to\mathrm{S0}})}$$

$$=\frac{[\mathrm{S_1}]k_{\mathrm{FL}}^{\mathrm{S1}\to\mathrm{S0}}}{[\mathrm{S_1}](k_{\mathrm{FL}}^{\mathrm{S1}\to\mathrm{S0}}+k_{\mathrm{IC}}^{\mathrm{S1}\to\mathrm{S0}})+[\mathrm{S_1}]\frac{k_{\mathrm{ISC}}^{\mathrm{S1}\to\mathrm{T1}}(k_{\mathrm{PH}}^{\mathrm{T1}\to\mathrm{S0}}+k_{\mathrm{ISC}}^{\mathrm{T1}\to\mathrm{S0}})}{(k_{\mathrm{PH}}^{\mathrm{T1}\to\mathrm{S0}}+k_{\mathrm{ISC}}^{\mathrm{T1}\to\mathrm{S0}}+k_{\mathrm{rISC}}^{\mathrm{T1}\to\mathrm{S1}})}}=\frac{k_{\mathrm{FL}}^{\mathrm{S1}\to\mathrm{S0}}}{(k_{\mathrm{FL}}^{\mathrm{S1}\to\mathrm{S0}}+k_{\mathrm{IC}}^{\mathrm{S1}\to\mathrm{S0}})+\frac{k_{\mathrm{ISC}}^{\mathrm{S1}\to\mathrm{T1}}(k_{\mathrm{PH}}^{\mathrm{T1}\to\mathrm{S0}}+k_{\mathrm{ISC}}^{\mathrm{T1}\to\mathrm{S0}})}{(k_{\mathrm{PH}}^{\mathrm{T1}\to\mathrm{S0}}+k_{\mathrm{ISC}}^{\mathrm{T1}\to\mathrm{S0}}+k_{\mathrm{rISC}}^{\mathrm{T1}\to\mathrm{S1}})}} \tag{S4.15}$$

Four-state (eq S4.3) and five-state (eq S4.4) models can follow a similar workflow to determine the PLQY of fluorescence.

5. Natural Transition Orbitals of DOBNA and DiKTa

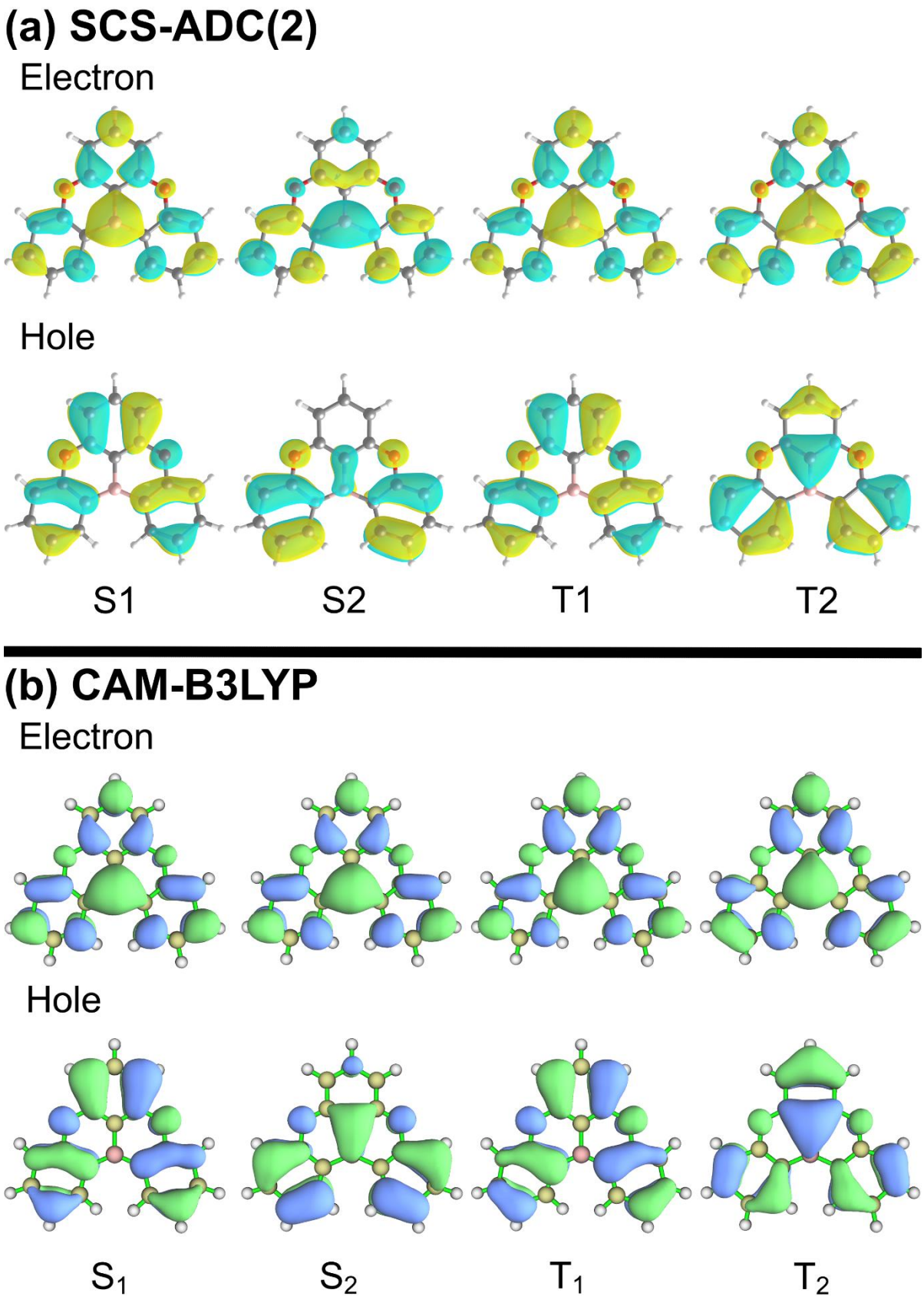

Figure S1. Natural transition orbitals (NTOs) of DOBNA at the ground-state geometry calculated by (a) SCS-ADC(2) and (b) TD(A)-CAM-B3LYP. Visualizations were generated using (a) VESTA[35] and (b) Multiwfn[36,37] (isovalue = 0.026).

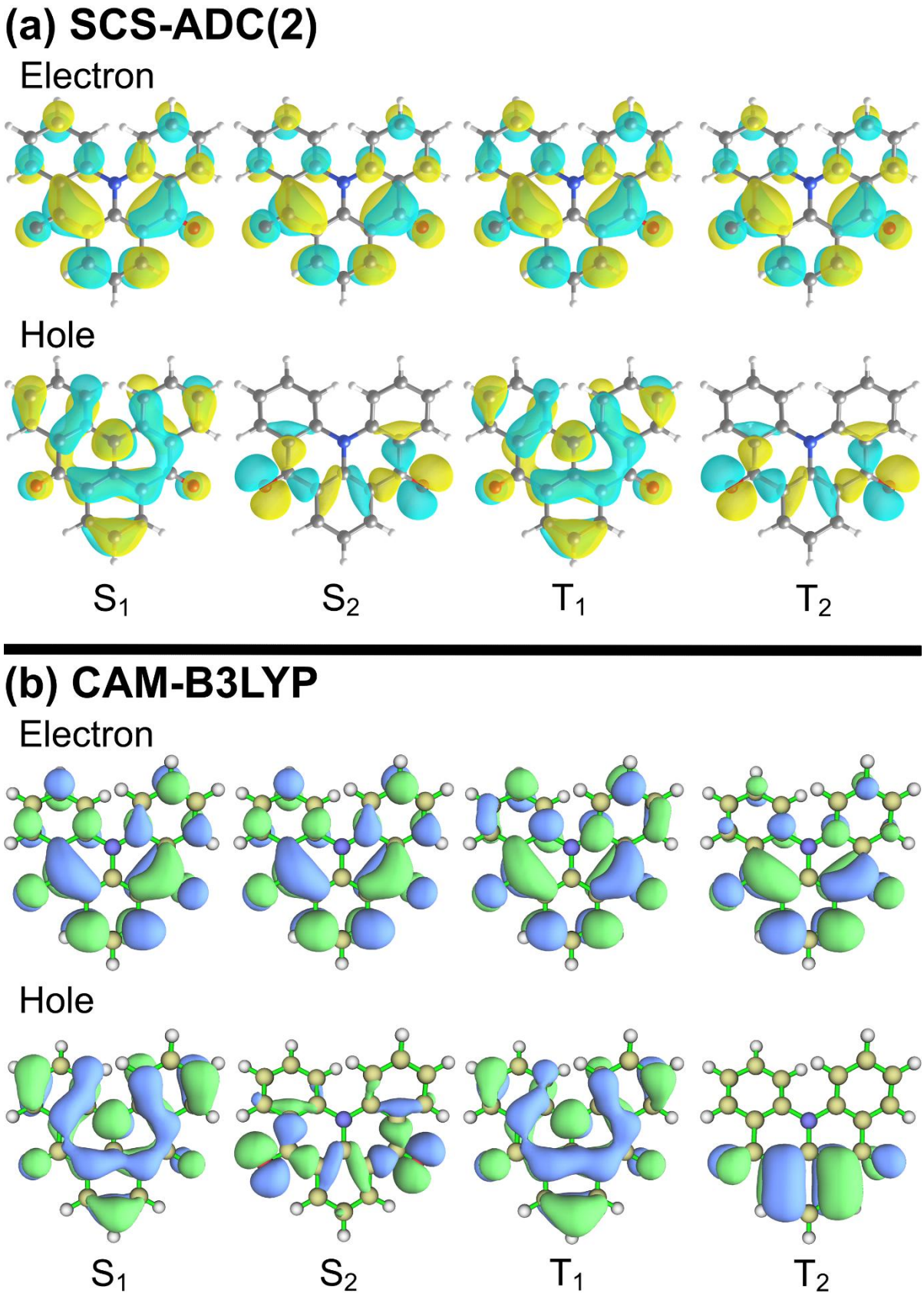

Figure S2. Natural transition orbitals (NTOs) of DiKTa at the ground-state geometry calculated by (a) SCS-ADC(2) and (b) TD(A)-CAM-B3LYP. Visualizations were generated using (a) VESTA and (b) Multiwfn (isovalue = 0.026).

6. Optimized Ground and Excited State Geometries

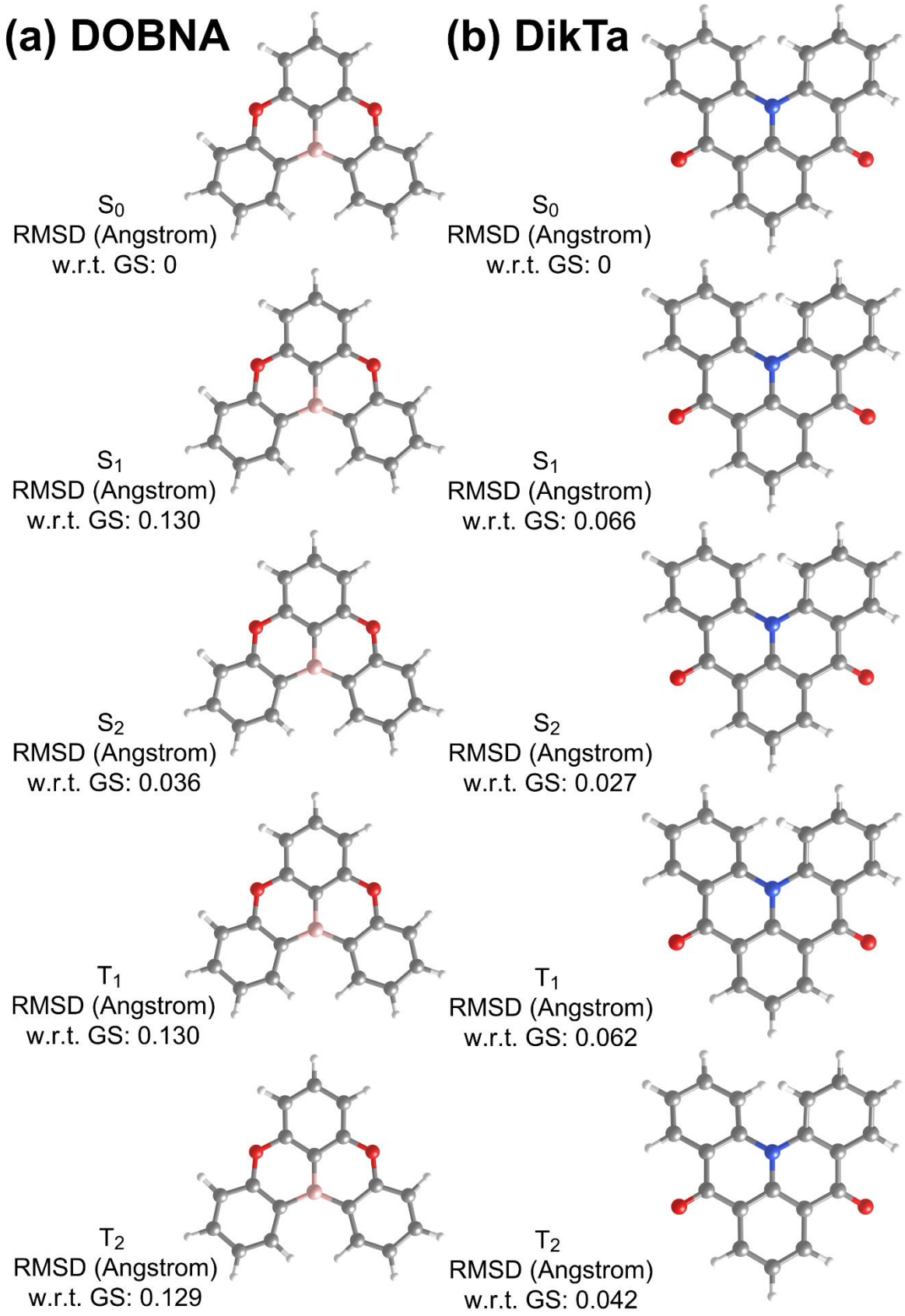

Figure S3. Optimized ground and excited state geometries of (a) DOBNA and (b) DiKTa at the TD(A)-CAM-B3LYP/6-311G(d,p) level. Blue: nitrogen, red: oxygen, pink: boron. Root Mean Square Deviations (RMSD) quantify the structural changes upon excitation with respect to (w.r.t) the ground state (GS).

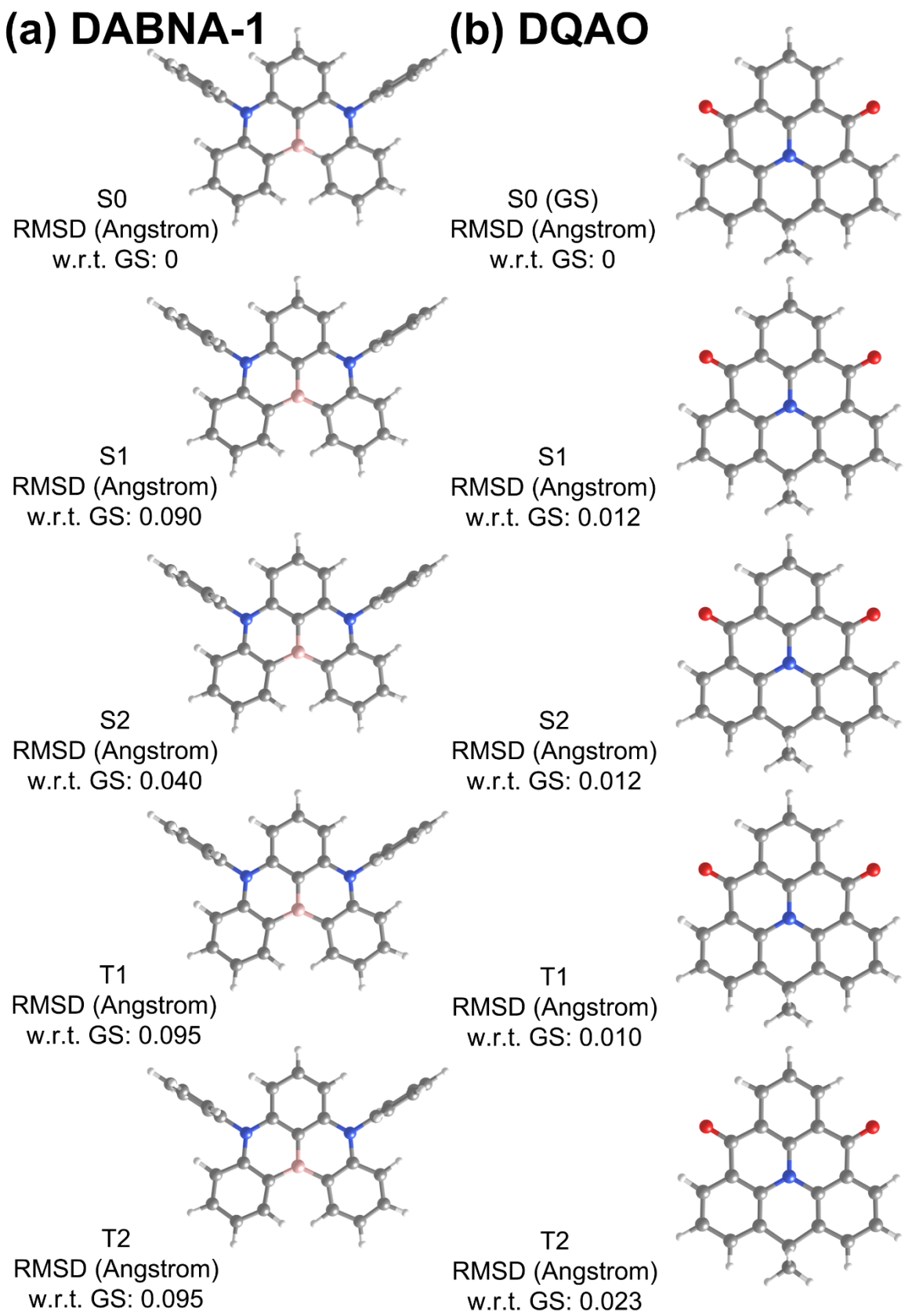

Figure S4. Optimized ground and excited state geometries of (a) DABNA-1 and (b) DQAO at the TD(A)-CAM-B3LYP/6-31(1)G(d,p) level. Blue: nitrogen, red: oxygen, pink: boron. Root Mean Square Deviations (RMSD) quantify the structural changes upon excitation with respect to (w.r.t) the ground state (GS).

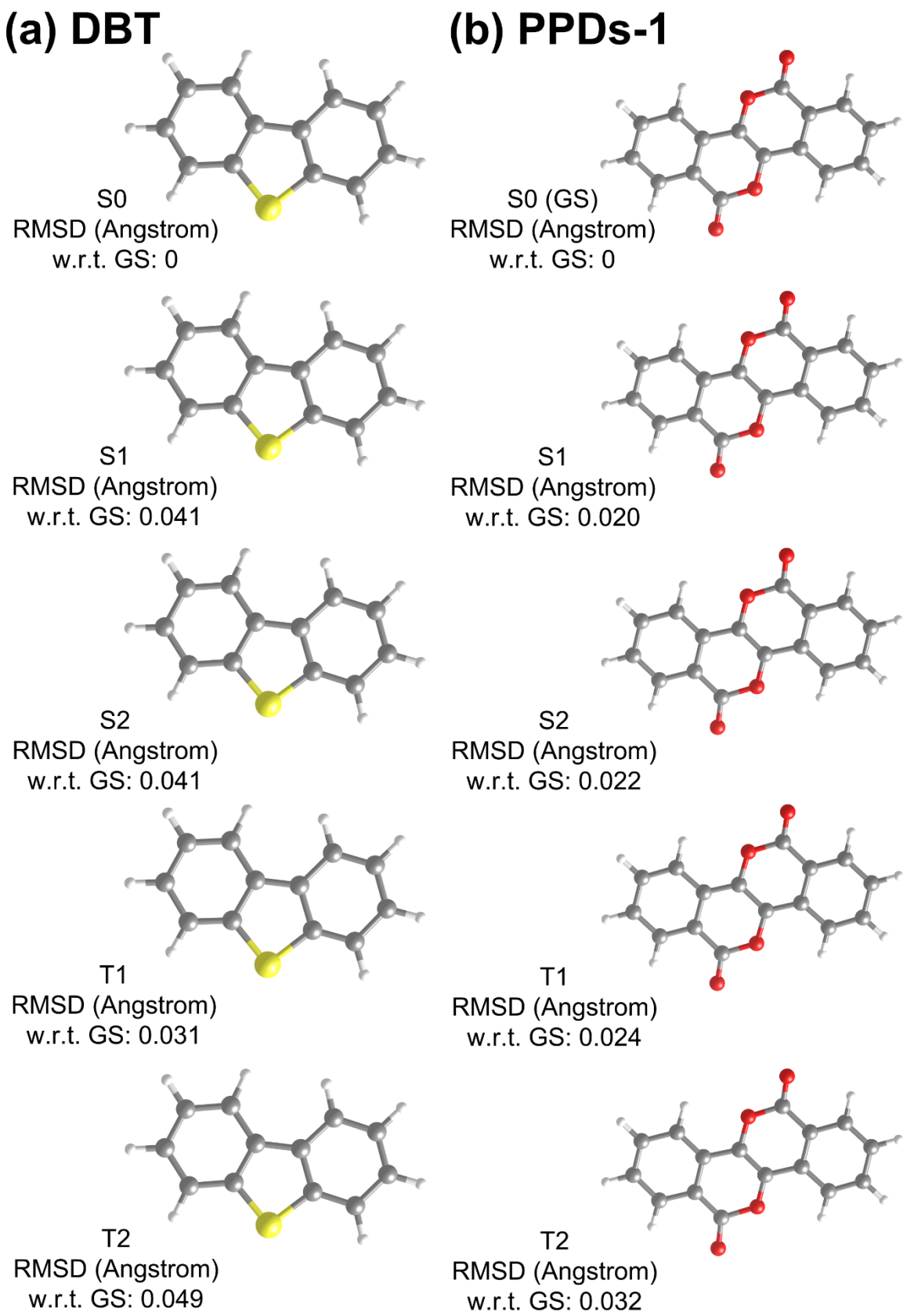

Figure S5. Optimized ground and excited state geometries of (a) DBT and (b) PPDs-1 at the TD(A)-CAM-B3LYP/6-31G(d,p) level. Yellow: sulfur, red: oxygen. Root Mean Square Deviations (RMSD) quantify the structural changes upon excitation with respect to (w.r.t) the ground state (GS).

7. Adiabatic Excitation Energies

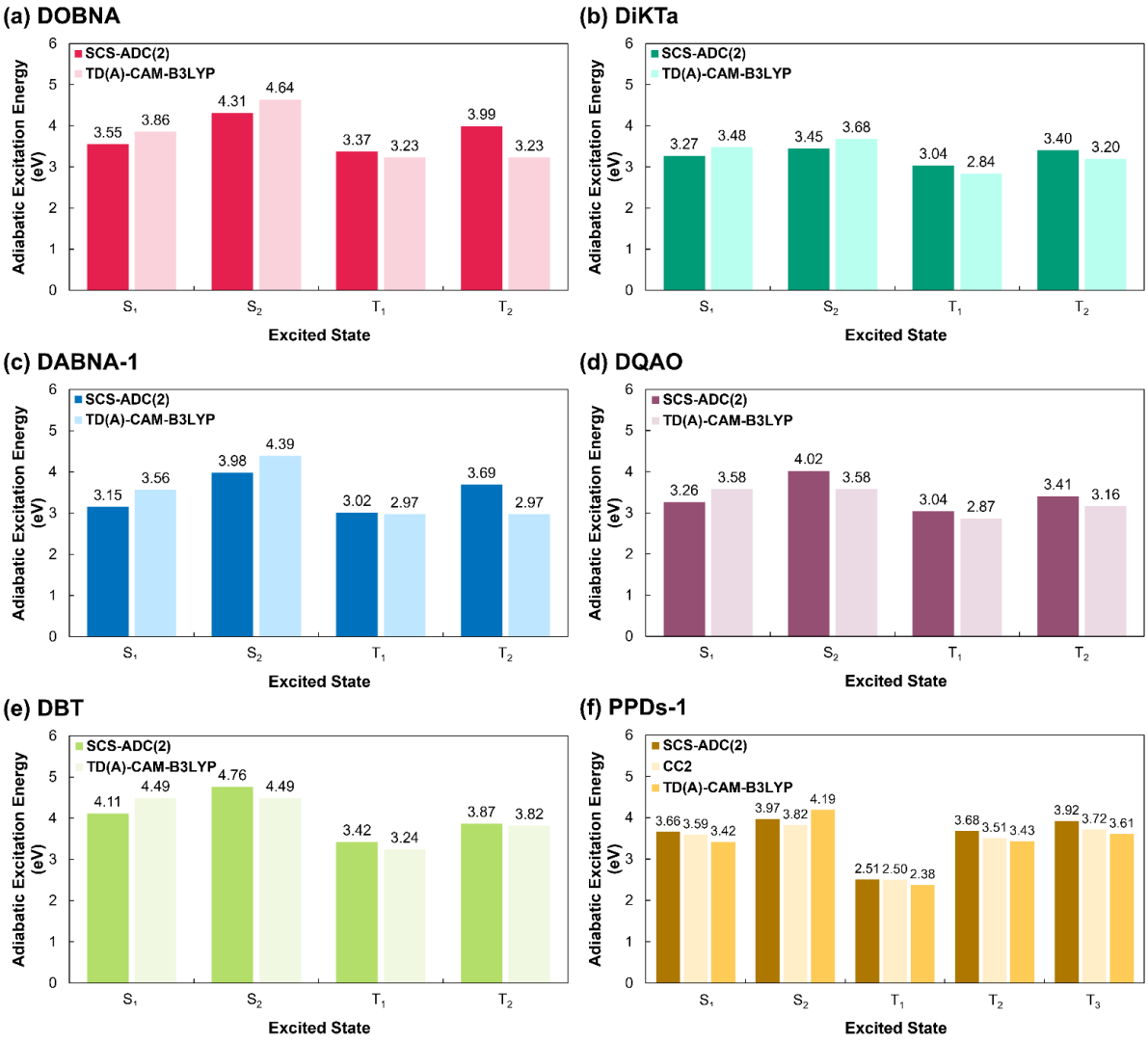

Figure S6. Adiabatic excitation energies (eV) for the excited states calculated at the TD(A)-CAM-B3LYP and SCS-ADC(2) levels for (a) DOBNA (red), (b) DiKTa (green), (c) DABNA-1 (blue), (d) DQAO (purple), (e) DBT (light green) and (f) PPDs-1 (orange).

8. Detailed Rate Constants Calculations of DOBNA and DiKTa

Table S1. ISC rate constants for the individual sublevels (Ms = 0, ±1) of DOBNA[a]

ISC Transition	Sublevel (Ms)	Rate (1/s)
$S_1 \rightarrow T_1$	0	2.24×10^{4}
$S_1 \rightarrow T_1$	±1	5.94×10^{5}
$S_1 \rightarrow T_2$	0	7.77×10^{2}
$S_1 \rightarrow T_2$	±1	1.08×10^{5}
$S_2 \rightarrow T_1$	0	1.33×10^{4}
$S_2 \rightarrow T_1$	±1	5.38×10^{6}
$S_2 \rightarrow T_2$	0	6.78×10^{5}
$S_2 \rightarrow T_2$	±1	2.44×10^{7}
$T_1 \rightarrow S_0$	0	8.71×10^{3}
$T_1 \rightarrow S_0$	±1	2.15×10^{5}
$T_1 \rightarrow S_1$	0	7.70×10^{1}
$T_1 \rightarrow S_1$	±1	5.32×10^{3}
$T_1 \rightarrow S_2$	0	3.83×10^{2}
$T_1 \rightarrow S_2$	±1	4.77×10^{3}
$T_2 \rightarrow S_1$	0	1.26×10^{5}
$T_2 \rightarrow S_1$	±1	2.15×10^{6}
$T_2 \rightarrow S_2$	0	7.23×10^{1}
$T_2 \rightarrow S_2$	±1	1.90×10^{4}

[a]The total ISC rate constant for one singlet-to-triplet transition is obtained by summing the rate constants of the three triplet sublevels, whereas the total rISC rate constant for one triplet-to-singlet transition is calculated as the average over these sublevels.

Table S2. ISC rate constants for the individual sublevels (Ms = 0, ±1) of DiKTa[a]

ISC Transition	Sublevel	Rate (1/s)
$S_1 \rightarrow T_1$	0	3.39×10^{8}
$S_1 \rightarrow T_1$	±1	5.15×10^{9}
$S_1 \rightarrow T_2$	0	8.84×10^{8}
$S_1 \rightarrow T_2$	±1	3.05×10^{9}
$S_2 \rightarrow T_1$	0	2.76×10^{10}
$S_2 \rightarrow T_1$	±1	1.28×10^{11}
$S_2 \rightarrow T_2$	0	1.30×10^{11}
$S_2 \rightarrow T_2$	±1	3.95×10^{11}
$T_1 \rightarrow S_0$	0	1.22×10^{4}
$T_1 \rightarrow S_0$	±1	4.23×10^{4}
$T_1 \rightarrow S_1$	0	2.69×10^{5}
$T_1 \rightarrow S_1$	±1	1.91×10^{6}
$T_1 \rightarrow S_2$	0	6.82×10^{4}
$T_1 \rightarrow S_2$	±1	4.05×10^{5}
$T_2 \rightarrow S_1$	0	4.63×10^{8}
$T_2 \rightarrow S_1$	±1	3.30×10^{9}
$T_2 \rightarrow S_2$	0	1.21×10^{7}
$T_2 \rightarrow S_2$	±1	7.22×10^{7}

[a]The total ISC rate constant for one singlet-to-triplet transition is obtained by summing the rate constants of the three triplet sublevels, whereas the total rISC rate constant for one triplet-to-singlet transition is calculated as the average over these sublevels.

Table S3. Phosphorescence rate constants for the individual sublevels (Ms = 0, ±1)[a]

Molecule	Sublevel	Rate (1/s)
DOBNA	0	9.02×10^{-2}
DOBNA	1	4.97×10^{-2}
DOBNA	-1	1.55×10^{-1}
DiKTa	0	8.00×10^{-1}
DiKTa	1	4.02×10^{0}
DiKTa	-1	1.17×10^{-2}

[a]The total phosphorescence rate constant is calculated as the average over these sublevels.

Table S4. Reorganization energies for ISC transitions in DOBNA

ISC Transition	Reorganization Energy (cm^{-1})	Reorganization Energy (eV)
$S_1\rightarrow T_1$	145.48	0.02
$S_1\rightarrow T_2$	145.31	0.02
$S_2\rightarrow T_1$	1185.07	0.15
$S_2\rightarrow T_2$	1178.94	0.15
$T_1\rightarrow S_0$	697.74	0.09
$T_1\rightarrow S_1$	172.32	0.02
$T_1\rightarrow S_2$	1012.63	0.13
$T_2\rightarrow S_1$	172.18	0.02
$T_2\rightarrow S_2$	1015.26	0.13

Table S5. Reorganization energies for ISC transitions in DiKTa

ISC Transition	Reorganization Energy (1/cm)	Reorganization Energy (eV)
$S_1\rightarrow T_1$	186.73	0.02
$S_1\rightarrow T_2$	2085.2	0.26
$S_2\rightarrow T_1$	5628.08	0.70
$S_2\rightarrow T_2$	4876.38	0.60
$T_1\rightarrow S_0$	847.07	0.11
$T_1\rightarrow S_1$	194.99	0.02
$T_1\rightarrow S_2$	953.82	0.12
$T_2\rightarrow S_1$	1526.58	0.19
$T_2\rightarrow S_2$	2629.44	0.33

Table S6. SOCMEs at the Franck-Condon (FC) geometry for ISC transitions in DOBNA

ISC Transition	Sublevel	FC SOCME (cm^{-1})
$S_1\rightarrow T_1$	0	1.07×10^{-6}
$S_1\rightarrow T_1$	±1	1.74×10^{-4}
$S_1\rightarrow T_2$	0	2.99×10^{-2}
$S_1\rightarrow T_2$	±1	5.32×10^{-4}
$S_2\rightarrow T_1$	0	2.25×10^{-2}
$S_2\rightarrow T_1$	±1	6.81×10^{-4}
$S_2\rightarrow T_2$	0	2.07×10^{-5}
$S_2\rightarrow T_2$	±1	1.30×10^{-4}

$T_1 \rightarrow S_0$	0	1.60×10^{-2}
$T_1 \rightarrow S_0$	±1	1.60×10^{-1}
$T_1 \rightarrow S_1$	0	1.35×10^{-6}
$T_1 \rightarrow S_1$	±1	1.77×10^{-4}
$T_1 \rightarrow S_2$	0	5.89×10^{-2}
$T_1 \rightarrow S_2$	±1	1.63×10^{-1}
$T_2 \rightarrow S_1$	0	3.42×10^{-2}
$T_2 \rightarrow S_1$	±1	7.32×10^{-4}
$T_2 \rightarrow S_2$	0	6.43×10^{-7}
$T_2 \rightarrow S_2$	±1	1.98×10^{-1}

Table S7. SOCMEs at the Franck-Condon (FC) geometry for ISC transitions in DiKTa

ISC Transition	Sublevel	FC SOCME (cm^{-1})
$S_1 \rightarrow T_1$	0	7.84×10^{-5}
$S_1 \rightarrow T_1$	±1	1.16×10^{0}
$S_1 \rightarrow T_2$	0	5.65×10^{0}
$S_1 \rightarrow T_2$	±1	9.88×10^{0}
$S_2 \rightarrow T_1$	0	2.90×10^{-3}
$S_2 \rightarrow T_1$	±1	8.16×10^{0}
$S_2 \rightarrow T_2$	0	5.85×10^{0}
$S_2 \rightarrow T_2$	±1	1.07×10^{1}
$T_1 \rightarrow S_0$	0	7.83×10^{-1}
$T_1 \rightarrow S_0$	±1	4.74×10^{-1}
$T_1 \rightarrow S_1$	0	9.83×10^{-5}
$T_1 \rightarrow S_1$	±1	5.13×10^{-1}
$T_1 \rightarrow S_2$	0	4.64×10^{-1}
$T_1 \rightarrow S_2$	±1	9.39×10^{-1}
$T_2 \rightarrow S_1$	0	3.65×10^{-1}
$T_2 \rightarrow S_1$	±1	1.01×10^{0}
$T_2 \rightarrow S_2$	0	2.23×10^{0}
$T_2 \rightarrow S_2$	±1	8.03×10^{0}

Table S8. Franck-Condon (FC) and Herzberg-Teller (HT) contributions to the ISC transitions of DOBNA

ISC Transition	Sublevel	FC Component (%)	HT Component (%)
$S_1 \rightarrow T_1$	0	0	100
$S_1 \rightarrow T_1$	±1	0	100
$S_1 \rightarrow T_2$	0	34.17	65.83
$S_1 \rightarrow T_2$	±1	0	100
$S_2 \rightarrow T_1$	0	57.31	42.69
$S_2 \rightarrow T_1$	±1	0	100
$S_2 \rightarrow T_2$	0	0	100
$S_2 \rightarrow T_2$	±1	0	100
$T_1 \rightarrow S_0$	0	0.14	99.86
$T_1 \rightarrow S_0$	±1	0.58	99.42
$T_1 \rightarrow S_1$	0	0	100
$T_1 \rightarrow S_1$	±1	0	100

$T_1 \rightarrow S_2$	0	34.14	65.86
$T_1 \rightarrow S_2$	±1	20.92	79.08
$T_2 \rightarrow S_1$	0	3.3	96.7
$T_2 \rightarrow S_1$	±1	0	100
$T_2 \rightarrow S_2$	0	0	100
$T_2 \rightarrow S_2$	±1	42.29	57.71

Table S9. Franck-Condon (FC) and Herzberg-Teller (HT) contributions to the ISC transitions of DiKTa

ISC Transition	Sublevel	FC Component (%)	HT Component (%)
$S_1 \rightarrow T_1$	0	0	100
$S_1 \rightarrow T_1$	±1	0.91	99.09
$S_1 \rightarrow T_2$	0	4.54	95.46
$S_1 \rightarrow T_2$	±1	4.03	95.97
$S_2 \rightarrow T_1$	0	0	100
$S_2 \rightarrow T_1$	±1	1.58	98.42
$S_2 \rightarrow T_2$	0	5.58	94.42
$S_2 \rightarrow T_2$	±1	6.19	93.81
$T_1 \rightarrow S_0$	0	40.01	59.99
$T_1 \rightarrow S_0$	±1	4.22	95.78
$T_1 \rightarrow S_1$	0	0	100
$T_1 \rightarrow S_1$	±1	8.77	91.23
$T_1 \rightarrow S_2$	0	22.03	77.97
$T_1 \rightarrow S_2$	±1	15.17	84.83
$T_2 \rightarrow S_1$	0	7.48	92.52
$T_2 \rightarrow S_1$	±1	7.95	92.05
$T_2 \rightarrow S_2$	0	51.74	48.26
$T_2 \rightarrow S_2$	±1	112.32	-12.32

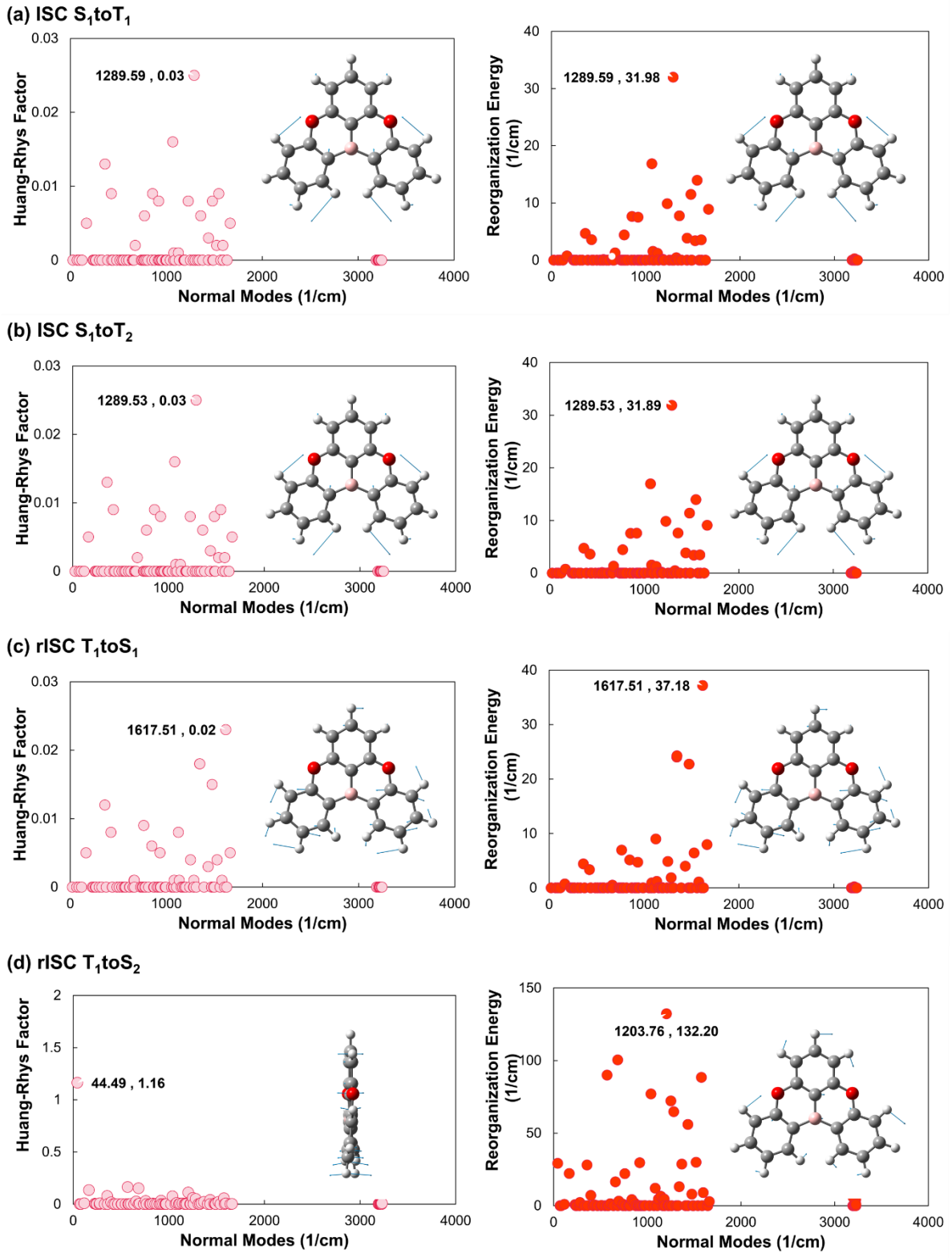

Figure S7. Huang-Rhys (HR) factors (left) and reorganization energies (right) as functions of vibrational normal modes for DOBNA: (a) ISC ($S_1 \rightarrow T1$), (b) ISC ($S_1 \rightarrow T_2$), (c) rISC ($T_1 \rightarrow S_1$), and (d) rISC ($T_1 \rightarrow S_2$). The highest HR factor and reorganization energy with their corresponding frequencies are indicated. The inset shows the displacement vectors of the normal modes corresponding to the highest HR factor (left) and reorganization energy (right).

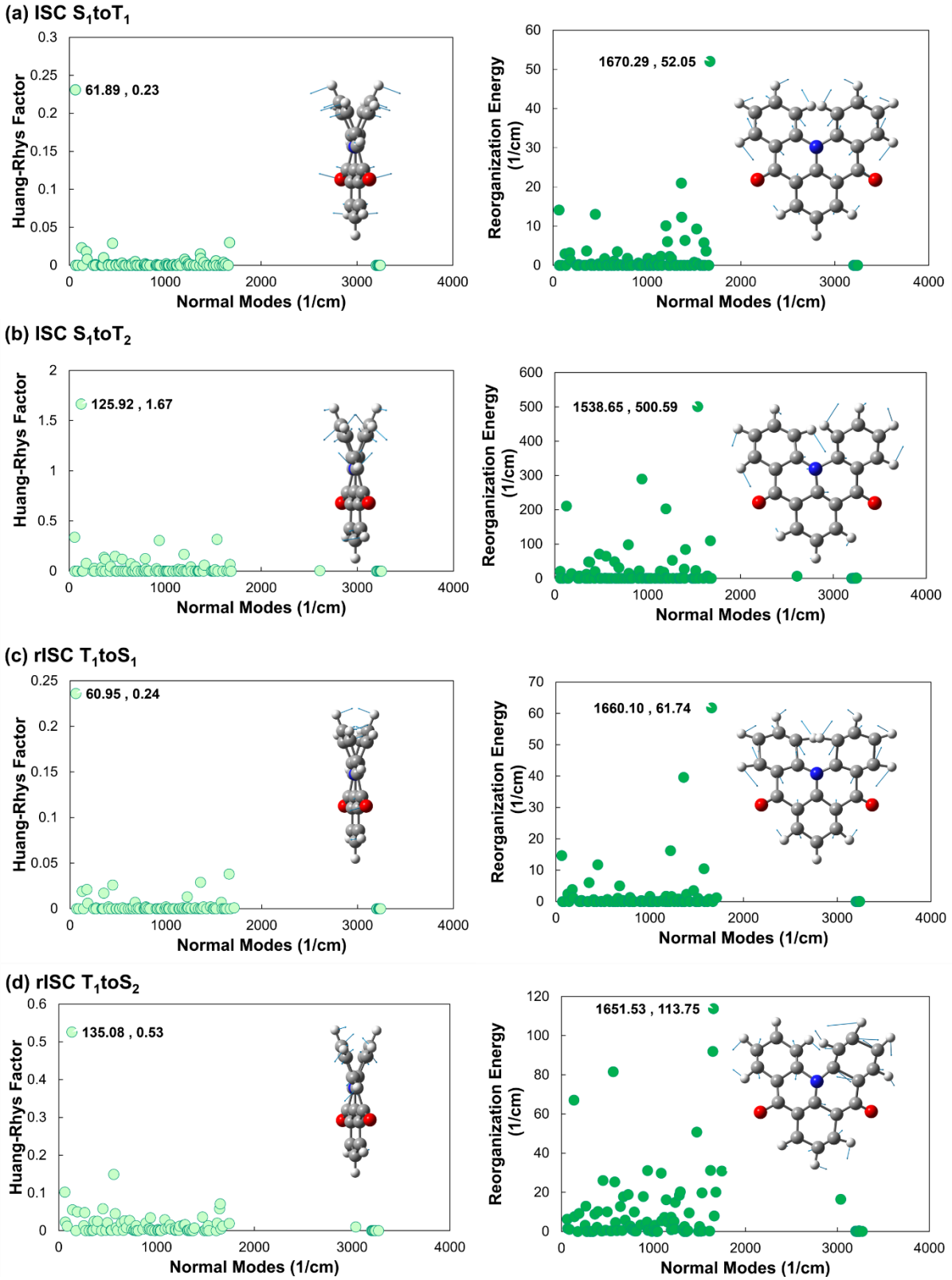

Figure S8. Huang-Rhys (HR) factors and reorganization energies as functions of vibrational normal modes for DiKTa: (a) ISC ($S_1 \rightarrow T_1$), (b) ISC ($S_1 \rightarrow T_2$), (c) rISC ($T_1 \rightarrow S_1$), and (d) rISC ($T_1 \rightarrow S_2$). The highest HR factor and reorganization energy with their corresponding frequencies are indicated. The inset shows the displacement vectors of the normal modes corresponding to the highest HR factor (left) and reorganization energy (right).

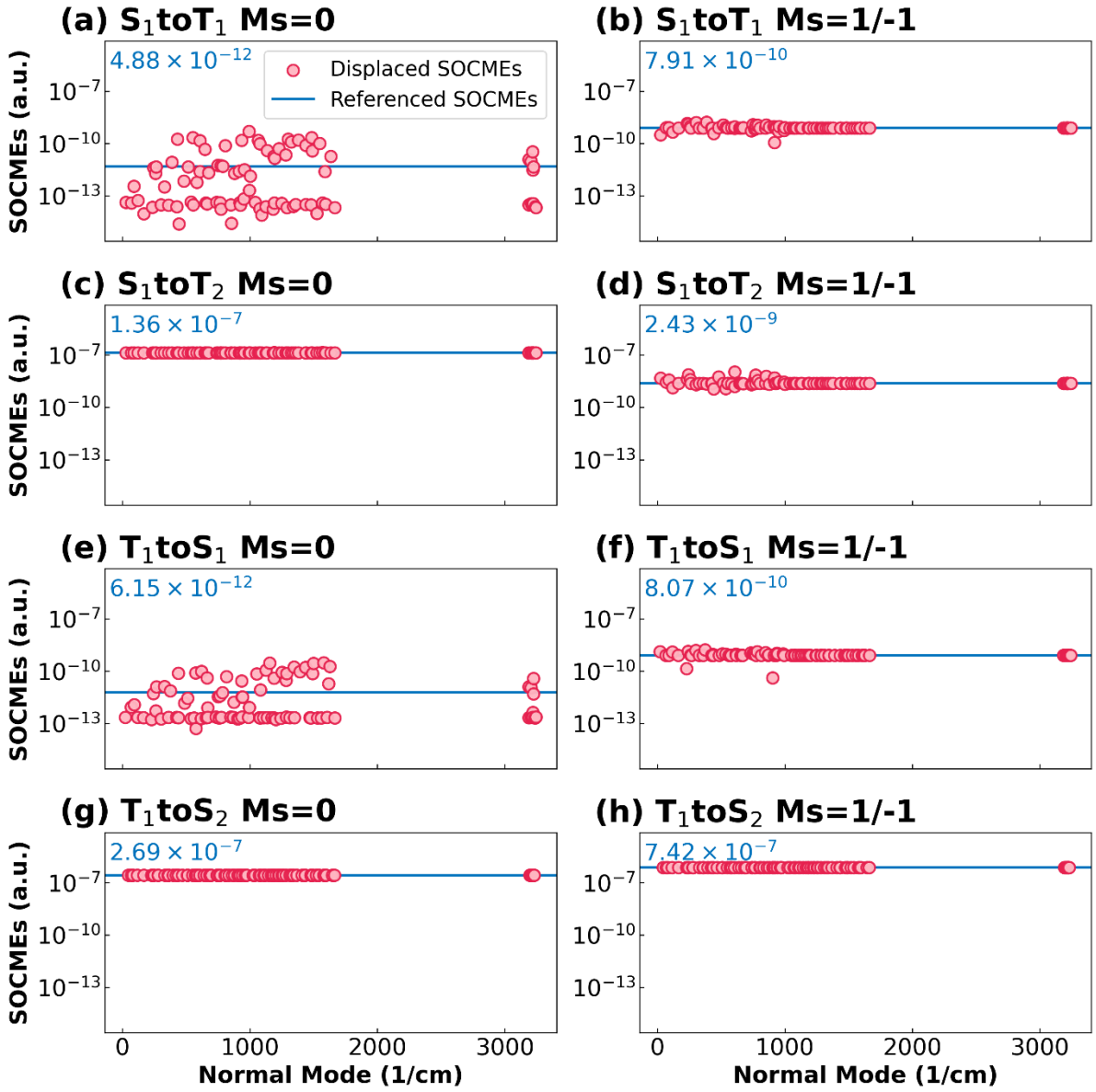

Figure S9. SOCMEs at the reference Franck-Condon (FC) geometry (blue) and displaced geometry (red) as functions of vibrational normal modes for DOBNA: (a-b) ISC $S_1 \rightarrow T_1$ (Ms=0) (Ms=1/-1), (c-d) ISC $S_1 \rightarrow T_2$ (Ms=0) (Ms=1/-1), (e-f) rISC $T_1 \rightarrow S_1$ (Ms=0) (Ms=1/-1), and (g-h) rISC $T_1 \rightarrow S_2$ (Ms=0) (Ms=1/-1). The SOCMEs values at the reference FC geometry are indicated (blue).

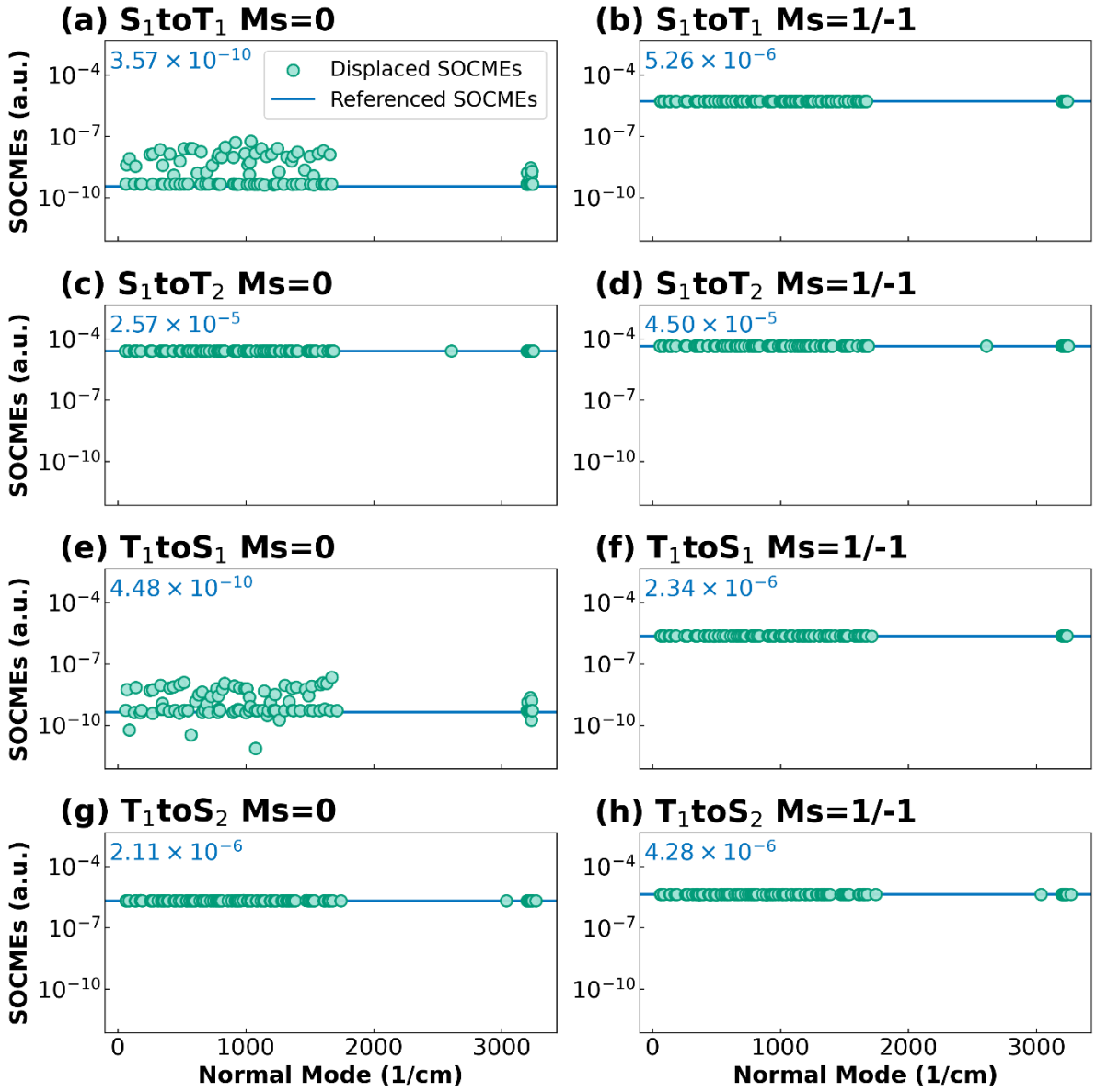

Figure S10. SOCMEs at the reference Franck-Condon (FC) geometry (blue) and displaced geometries (green) as functions of vibrational normal modes for DiKTa: (a-b) ISC S1⟶T1 (Ms=0) (Ms=1/-1), (c-d) ISC S1⟶T2 (Ms=0) (Ms=1/-1), (e-f) rISC T1⟶S1 (Ms=0) (Ms=1/-1), and (g-h) rISC T1⟶S2 (Ms=0) (Ms=1/-1). The SOCMEs values at the reference FC geometry are indicated (blue).

9. Rate Constants Calculations of DABNA-1, DQAO, DBT and PPDs-1

Table S10. Calculated rate constant (s^{-1}) for all transitions considered in DABNA-1, DQAO, DBT and PPDs-1

Transition	Type	DABNA-1	DQAO	DBT	PPDs-1
$S_1 \rightarrow T_1$	ISC	8.30×10^{6}	2.72×10^{9}	2.13×10^{8}	4.61×10^{3}
$S_1 \rightarrow T_2$	ISC	8.27×10^{4}	4.52×10^{7}	2.65×10^{8}	4.07×10^{7}
$S_1 \rightarrow T_3$	ISC	-	-	-	7.36×10^{4}
$S_2 \rightarrow T_1$	ISC	3.13×10^{6}	3.96×10^{9}	5.79×10^{4}	3.95×10^{7}
$S_2 \rightarrow T_2$	ISC	8.23×10^{7}	2.54×10^{11}	3.69×10^{7}	3.98×10^{7}
$S_2 \rightarrow T_3$	ISC	-	-	-	9.87×10^{5}
$T_1 \rightarrow S_0$	ISC	2.00×10^{3}	9.42×10^{3}	3.83×10^{4}	4.92×10^{5}
$T_1 \rightarrow S_1$	rISC	2.41×10^{4}	5.43×10^{5}	-	-
$T_1 \rightarrow S_2$	rISC	3.87×10^{3}	2.50×10^{8}	-	-
$T_2 \rightarrow S_1$	rISC	1.25×10^{6}	1.61×10^{9}	-	-
$T_2 \rightarrow S_2$	rISC	6.15×10^{3}	1.42×10^{8}	-	-
$S_1 \rightarrow S_0$	EM	9.05×10^{7}	6.46×10^{7}	4.75×10^{7}	3.74×10^{8}
$T_1 \rightarrow S_0$	EM	1.58×10^{-1}	2.36×10^{2}	7.57×10^{-1}	5.55×10^{-1}
$S_1 \rightarrow S_0$	IC	2.02×10^{7}	1.88×10^{7}	1.73×10^{7}	1.67×10^{7}
$S_2 \rightarrow S_0$	IC	5.88×10^{6}	1.12×10^{6}	1.87×10^{6}	3.86×10^{10}
$S_2 \rightarrow S_1$	IC	1.85×10^{10}	1.17×10^{9}	1.35×10^{10}	$2.54\times10^{12}(\Delta E_{SCS-ADC2}^{(S_2-S_1)})$ $4.37\times10^{12}(\Delta E_{cc2}^{(S_2-S_1)})$ $2.86\times10^{11}(\Delta E_{SCS-ADC2}^{(S_2-S_1)}$-0.2eV)
$T_2 \rightarrow T_1$	IC	1.92×10^{10}	1.05×10^{14}	8.80×10^{12}	5.75×10^{11}
$S_1 \rightarrow S_2$	rIC	2.30×10^{8}	2.17×10^{8}	5.11×10^{9}	$3.15\times10^{9}(\Delta E_{SCS-ADC2}^{(S_2-S_1)})$ $1.27\times10^{10}(\Delta E_{cc2}^{(S_1-S_2)})$ $6.49\times10^{10}(\Delta E_{SCS-ADC2}^{(S_2-S_1)}$-0.2eV)
$T_1 \rightarrow T_2$	rIC	1.07×10^{10}	3.97×10^{10}	7.04×10^{8}	2.14×10^{8}

Table S11. ISC rate constants for the individual sublevels (Ms = 0, ±1) in DABNA-1, DQAO, DBT and PPDs-1[a]

ISC Transition	Sublevel	DABNA-1	DQAO	DBT	PPDs-1
$S_1 \rightarrow T_1$	0	7.20×10^{5}	1.27×10^{9}	3.90×10^{5}	5.28×10^{2}
$S_1 \rightarrow T_1$	±1	3.79×10^{6}	7.20×10^{8}	1.06×10^{8}	2.04×10^{3}
$S_1 \rightarrow T_2$	0	1.89×10^{4}	4.39×10^{7}	9.20×10^{4}	4.50×10^{6}
$S_1 \rightarrow T_2$	±1	3.19×10^{4}	6.53×10^{5}	1.32×10^{8}	1.81×10^{7}
$S_1 \rightarrow T_3$	0	-	-	-	8.20×10^{3}
$S_1 \rightarrow T_3$	±1	-	-	-	3.27×10^{4}
$S_2 \rightarrow T_1$	0	9.72×10^{5}	3.92×10^{9}	1.23×10^{3}	1.01×10^{7}
$S_2 \rightarrow T_1$	±1	1.08×10^{6}	1.76×10^{7}	2.83×10^{4}	1.47×10^{7}
$S_2 \rightarrow T_2$	0	4.48×10^{7}	4.00×10^{10}	1.28×10^{5}	7.41×10^{6}
$S_2 \rightarrow T_2$	±1	1.87×10^{7}	1.07×10^{11}	1.84×10^{7}	1.62×10^{7}
$S_2 \rightarrow T_3$	0	-	-	-	6.03×10^{4}
$S_2 \rightarrow T_3$	±1	-	-	-	4.63×10^{5}
$T_1 \rightarrow S_0$	0	2.95×10^{3}	1.42×10^{4}	1.63×10^{2}	4.67×10^{5}
$T_1 \rightarrow S_0$	±1	1.52×10^{3}	7.04×10^{3}	5.74×10^{4}	5.04×10^{5}
$T_1 \rightarrow S_1$	0	1.51×10^{4}	9.57×10^{5}	-	-
$T_1 \rightarrow S_1$	±1	2.86×10^{4}	3.36×10^{5}	-	-

$T_1 \rightarrow S_2$	0	2.09×10^{3}	7.38×10^{8}	-	-
$T_1 \rightarrow S_2$	±1	4.77×10^{3}	6.38×10^{6}	-	-
$T_2 \rightarrow S_1$	0	2.38×10^{5}	3.73×10^{9}	-	-
$T_2 \rightarrow S_1$	±1	1.75×10^{6}	5.52×10^{8}	-	-
$T_2 \rightarrow S_2$	0	9.05×10^{3}	1.41×10^{8}	-	-
$T_2 \rightarrow S_2$	±1	4.70×10^{3}	1.42×10^{8}	-	-

[a]The total ISC rate constant for one singlet-to-triplet transition is obtained by summing the rate constants of the three triplet sublevels, whereas the total rISC rate constant for one triplet-to-singlet transition is calculated as the average over these sublevels.

Table S12. Phosphorescence rate constants for the individual sublevels (Ms = 0, ±1) in DABNA-1, DQAO, DBT and PPDs-1[a]

Sublevel	DABNA-1	DQAO	DBT	PPDs-1
0	4.18×10^{-1}	7.05×10^{2}	1.80×10^{0}	7.45×10^{-2}
1	1.10×10^{-2}	2.76×10^{0}	4.90×10^{-3}	1.04×10^{-1}
-1	4.40×10^{-2}	1.56×10^{-3}	4.61×10^{-1}	1.49×10^{0}

[a]The total phosphorescence rate constant is calculated as the average over these sublevels.

Table S13. Reorganization energies (cm^{-1}) for ISC transitions in DABNA-1, DQAO, DBT and PPDs-1

ISC Transition	DABNA-1	DQAO	DBT	PPDs-1
$S_1 \rightarrow T_1$	108.84	223.08	1984.15	235.45
$S_1 \rightarrow T_2$	108.79	1736.50	782.22	2306.24
$S_1 \rightarrow T_3$	-	-	-	1803.36
$S_2 \rightarrow T_1$	821.67	232.66	1985.98	2375.36
$S_2 \rightarrow T_2$	821.67	1737.40	782.60	503.30
$S_2 \rightarrow T_3$	-	-	-	320.07
$T_1 \rightarrow S_0$	542.04	658.16	2874.72	3174.33
$T_1 \rightarrow S_1$	114.62	228.35	-	-
$T_1 \rightarrow S_2$	826.90	236.97	-	-
$T_2 \rightarrow S_1$	114.58	1291.00	-	-
$T_2 \rightarrow S_2$	826.76	1295.43	-	-

Table S14. SOCMEs (cm^{-1}) at the Franck-Condon (FC) geometry for ISC transitions in DABNA-1, DQAO, DBT and PPDs-1

ISC Transition	Sublevel	DABNA-1	DQAO	DBT	PPDs-1
$S_1 \rightarrow T_1$	0	4.68×10^{-2}	1.73×10^{-4}	3.54×10^{-2}	1.38×10^{-2}
$S_1 \rightarrow T_1$	±1	1.24×10^{-5}	3.12×10^{-4}	5.32×10^{-5}	1.01×10^{-2}
$S_1 \rightarrow T_2$	0	6.65×10^{-5}	4.03×10^{-3}	1.50×10^{-4}	4.96×10^{-2}
$S_1 \rightarrow T_2$	±1	2.96×10^{-1}	1.36×10^{-2}	2.70×10^{-6}	4.18×10^{-2}
$S_1 \rightarrow T_3$	0	-	-	-	8.18×10^{-2}
$S_1 \rightarrow T_3$	±1	-	-	-	6.73×10^{-2}
$S_2 \rightarrow T_1$	0	1.98×10^{-1}	1.95×10^{0}	7.01×10^{-5}	2.52×10^{-4}
$S_2 \rightarrow T_1$	±1	9.21×10^{-5}	9.01×10^{0}	3.55×10^{-6}	4.68×10^{-4}
$S_2 \rightarrow T_2$	0	7.76×10^{-5}	2.24×10^{1}	7.12×10^{-3}	1.83×10^{-2}
$S_2 \rightarrow T_2$	±1	9.55×10^{-2}	6.54×10^{-2}	2.07×10^{-5}	1.65×10^{-2}
$S_2 \rightarrow T_3$	0	-	-	-	2.93×10^{-5}
$S_2 \rightarrow T_3$	±1	-	-	-	5.21×10^{-5}
$T_1 \rightarrow S_0$	0	6.35×10^{-5}	1.53×10^{-4}	1.83×10^{-2}	1.41×10^{-3}
$T_1 \rightarrow S_0$	±1	1.26×10^{-1}	3.38×10^{-2}	2.65×10^{-5}	1.05×10^{-3}
$T_1 \rightarrow S_1$	0	4.95×10^{-2}	1.71×10^{-4}	-	-

$T_1 \rightarrow S_1$	±1	4.04×10^{-6}	9.93×10^{-5}	-	-
$T_1 \rightarrow S_2$	0	3.28×10^{-5}	1.62×10^{-2}	-	-
$T_1 \rightarrow S_2$	±1	2.64×10^{-1}	8.22×10^{0}	-	-
$T_2 \rightarrow S_1$	0	3.12×10^{-5}	3.08×10^{-4}	-	-
$T_2 \rightarrow S_1$	±1	3.15×10^{-1}	4.80×10^{-2}	-	-
$T_2 \rightarrow S_2$	0	1.13×10^{-1}	2.33×10^{1}	-	-
$T_2 \rightarrow S_2$	±1	1.26×10^{-5}	6.40×10^{-2}	-	-

Table S15. Herzberg-Teller (HT) contributions (%) to the ISC transitions in DABNA-1, DQAO, DBT and PPDs-1

ISC Transition	Sublevel	DABNA-1	DQAO	DBT	PPDs-1
$S_1 \rightarrow T_1$	0	76.08	100	93.49	98.32
$S_1 \rightarrow T_1$	±1	100	100	100	99.77
$S_1 \rightarrow T_2$	0	100	100	100	94.02
$S_1 \rightarrow T_2$	±1	47.71	99.98	100	98.94
$S_1 \rightarrow T_3$	0	-	-	-	89.19
$S_1 \rightarrow T_3$	±1	-	-	-	98.16
$S_2 \rightarrow T_1$	0	95.02	99.99	100	100
$S_2 \rightarrow T_1$	±1	100	65.05	100	100
$S_2 \rightarrow T_2$	0	100	53.59	99.78	99.43
$S_2 \rightarrow T_2$	±1	90.39	100	100	99.79
$S_2 \rightarrow T_3$	0	-	-	-	100
$S_2 \rightarrow T_3$	±1	-	-	-	100
$T_1 \rightarrow S_0$	0	100	100	98.41	100
$T_1 \rightarrow S_0$	±1	92.03	99.85	100	100
$T_1 \rightarrow S_1$	0	48.44	100	-	-
$T_1 \rightarrow S_1$	±1	100	100	-	-
$T_1 \rightarrow S_2$	0	100	100	-	-
$T_1 \rightarrow S_2$	±1	21.67	47.26	-	-
$T_2 \rightarrow S_1$	0	100	100	-	-
$T_2 \rightarrow S_1$	±1	95.32	99.89	-	-
$T_2 \rightarrow S_2$	0	24.06	57.75	-	-
$T_2 \rightarrow S_2$	±1	100	100	-	-

10. Simulated Decay Kinetics of DABNA-1, DQAO, DBT and PPDs-1

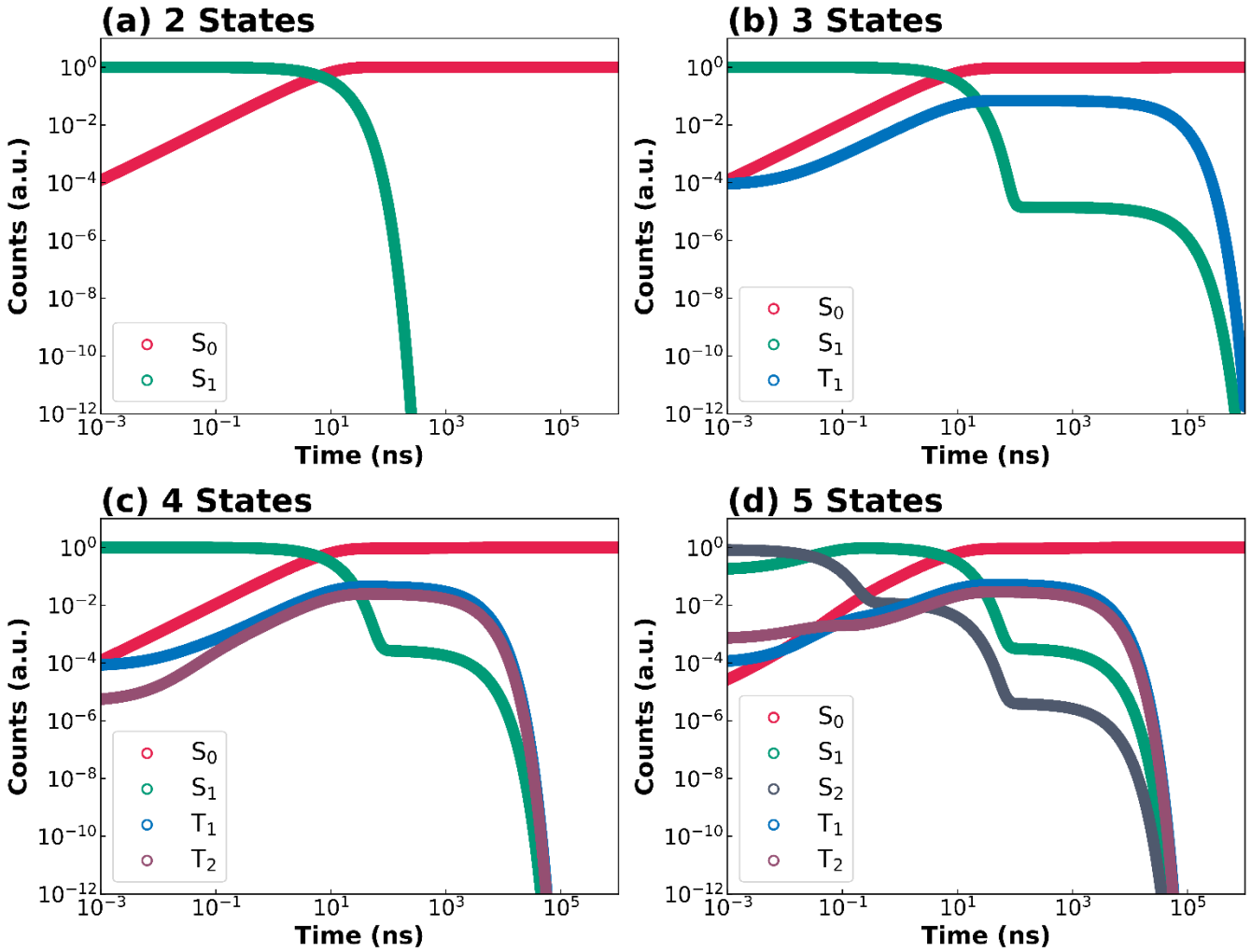

Figure S11. Simulated population decay kinetics of DABNA-1 over a 1 ms timescale based on (a) two-state (S_0, S_1), (b) three-state (S_0, S_1, T_1), (c) four-state (S_0, S_1, T_1, T_2), and (d) five-state (S_0, S_1, S_2, T_1, T_2) kinetic models. The number of absorbed photons is set to 1, with the excitation pulse width of 10 ps. Both time (x-axis) and population (y-axis) are plotted on logarithmic scales.

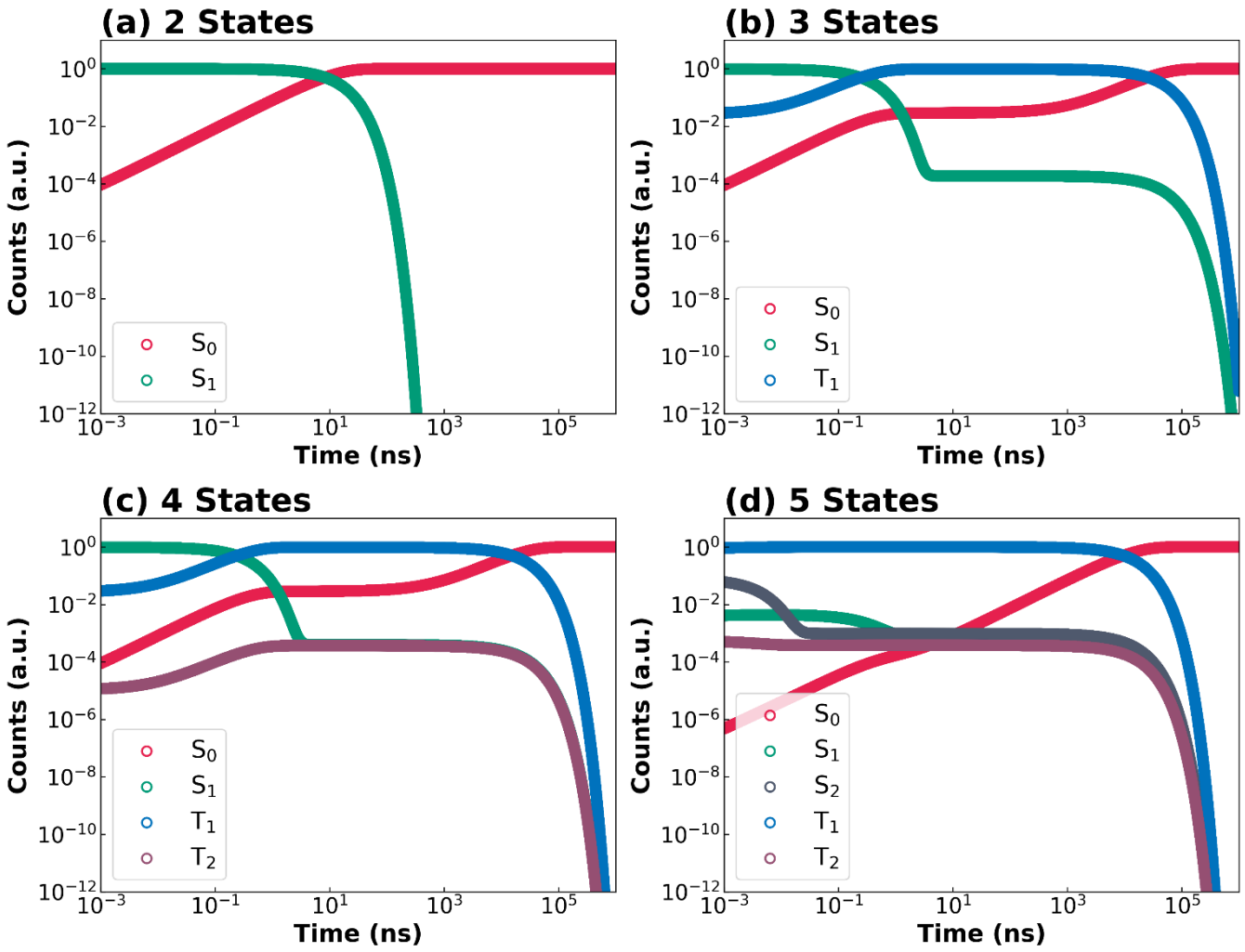

Figure S12. Simulated population decay kinetics of DQAO over a 1 ms timescale based on (a) two-state (S_0, S_1), (b) three-state (S_0, S_1, T_1), (c) four-state (S_0, S_1, T_1, T_2), and (d) five-state (S_0, S_1, S_2, T_1, T_2) kinetic models. The number of absorbed photons is set to 1, with the excitation pulse width of 10 ps. Both time (x-axis) and population (y-axis) are plotted on logarithmic scales.

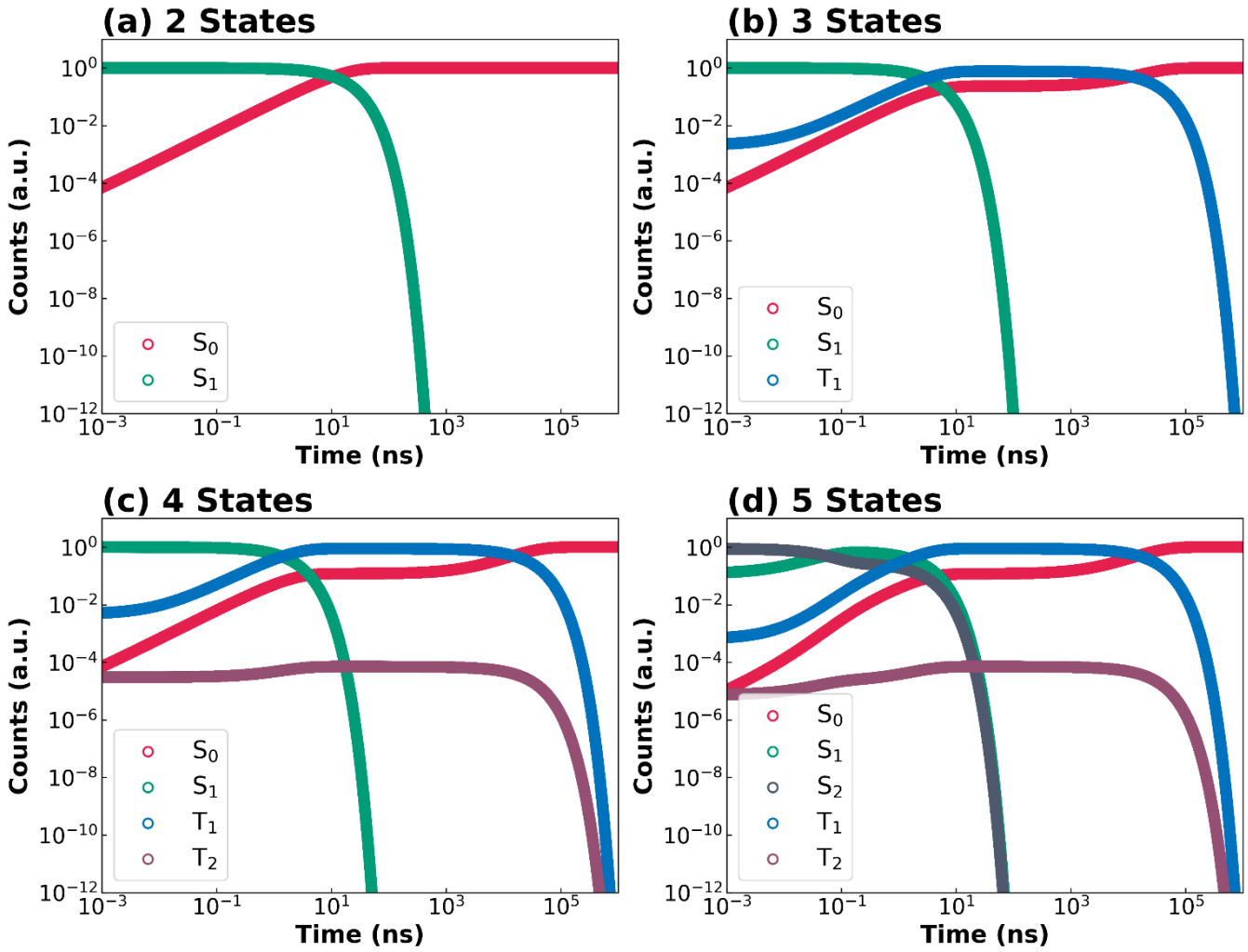

Figure S13. Simulated population decay kinetics of DBT over a 1 ms timescale based on (a) two-state (S_0, S_1), (b) three-state (S_0, S_1, T_1), (c) four-state (S_0, S_1, T_1, T_2), and (d) five-state (S_0, S_1, S_2, T_1, T_2) kinetic models. The number of absorbed photons is set to 1, with the excitation pulse width of 10 ps. Both time (x-axis) and population (y-axis) are plotted on logarithmic scale.

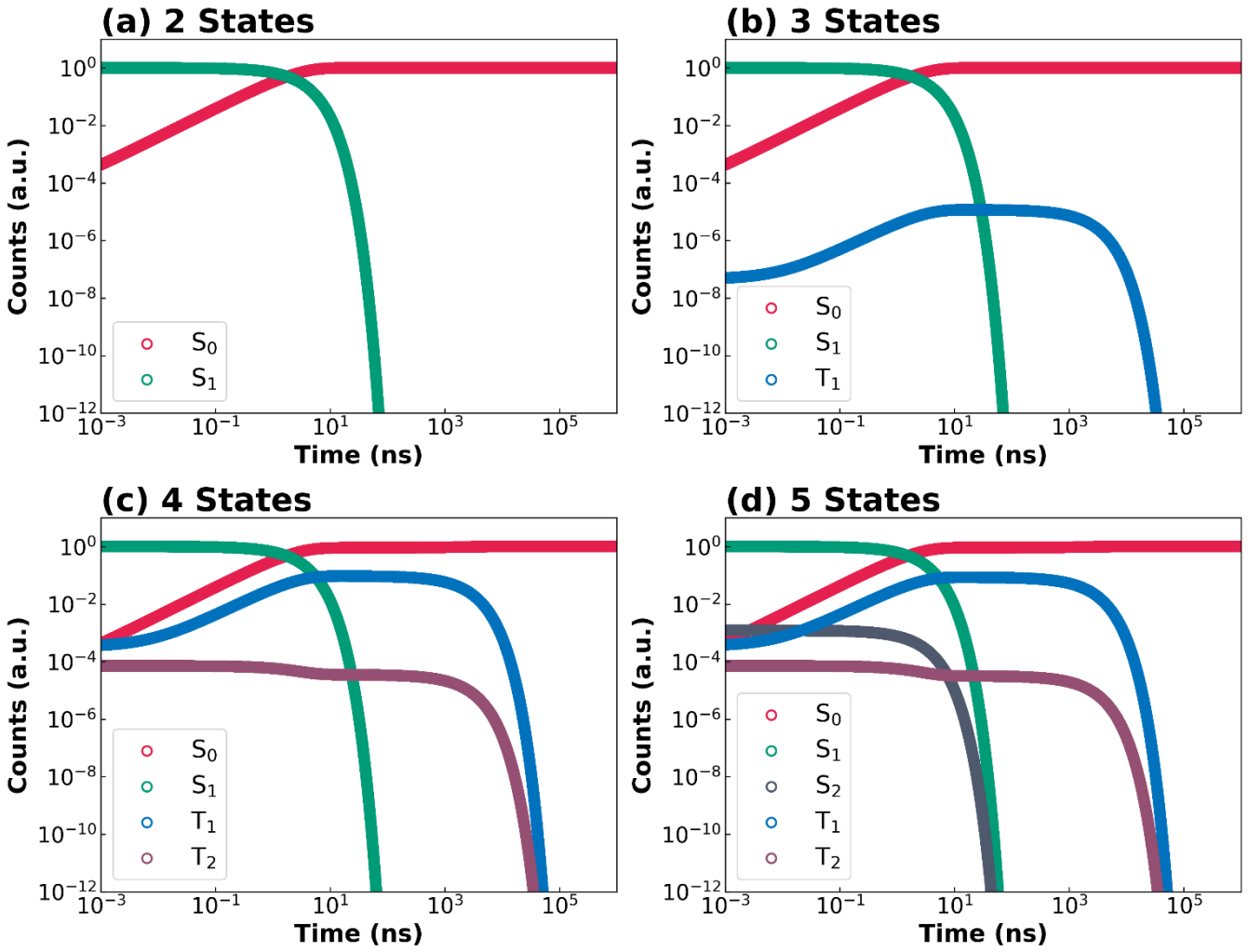

Figure S14. Simulated population decay kinetics of PPDs-1 over a 1 ms timescale based on (a) two-state (S_0, S_1), (b) three-state (S_0, S_1, T_1), (c) four-state (S_0, S_1, T_1, T_2), and (d) five-state (S_0, S_1, S_2, T_1, T_2) kinetic models. The number of absorbed photons is set to 1, with the excitation pulse width of 10 ps. Both time (x-axis) and population (y-axis) are plotted on logarithmic scales.

11. Error Diagnosis of Computational Rate Constants

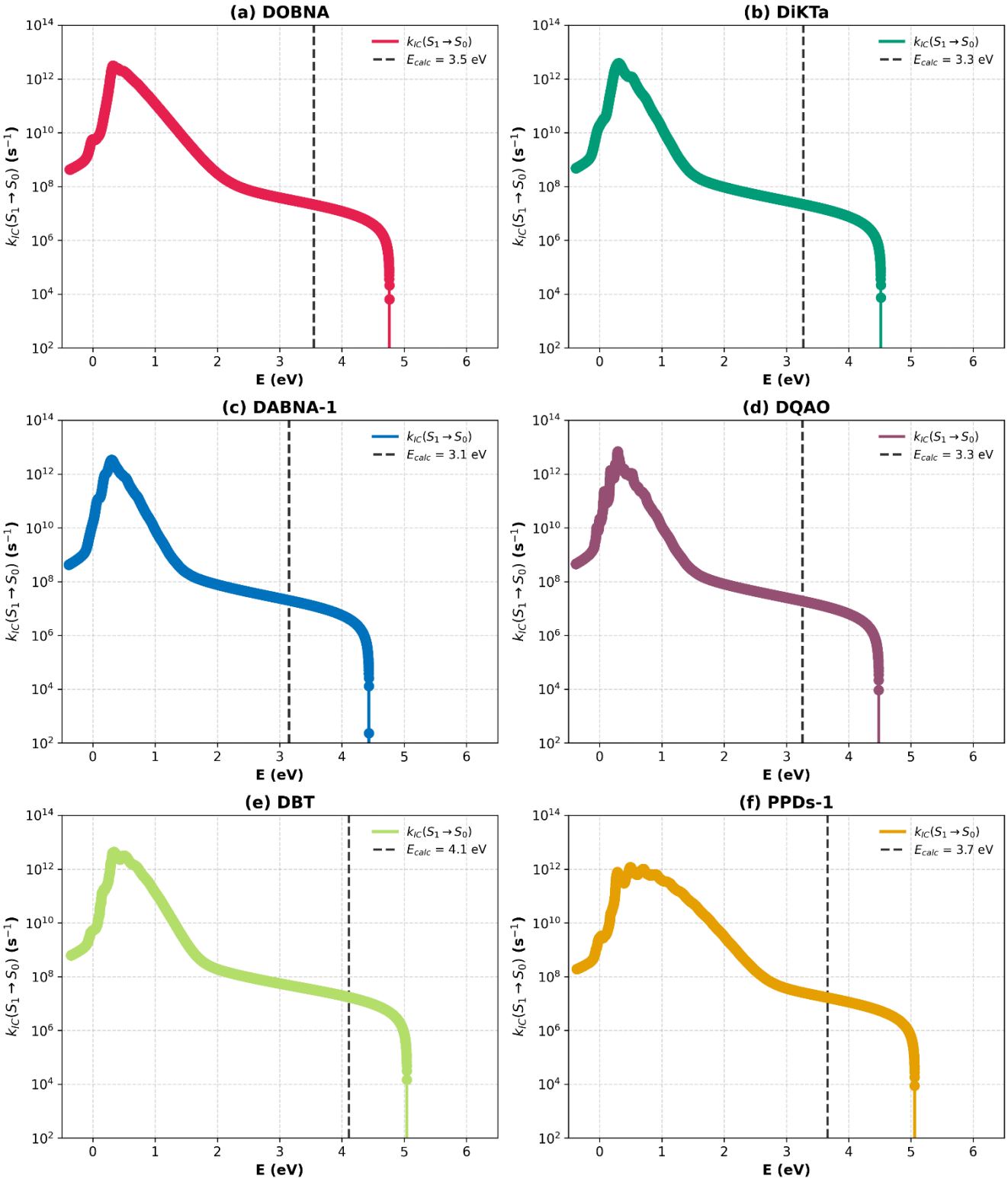

Figure S15. Dependencies of calculated rate constant IC $S_1 \rightarrow S_0$ on adiabatic energy gap for (a) DOBNA (red), (b) DiKTa (green), (c) DABNA-1 (blue) and (d) DQAO (purple), (e) DBT (light green), (f) PPDs-1 (orange).

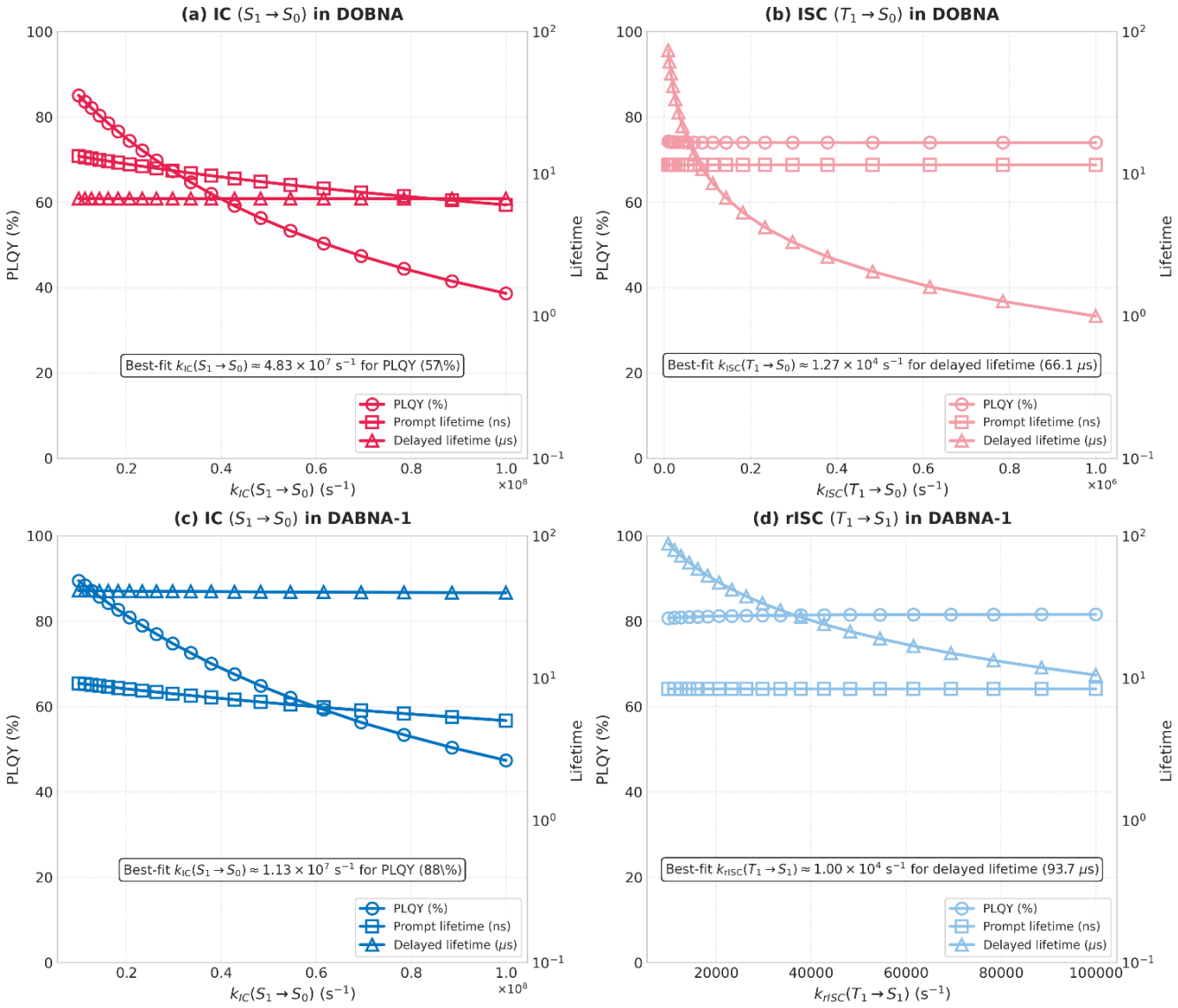

Figure S16. Influences of calculated rate constant IC $S_1 \rightarrow S_0$ in DOBNA (red) (a), ISC $T_1 \rightarrow S_0$ in DOBNA (light red) (b), IC $S_1 \rightarrow S_0$ in DABNA-1 (blue) (c) and rISC $T_1 \rightarrow S_0$ in DABNA-1 (light blue) (d) with three-state model.

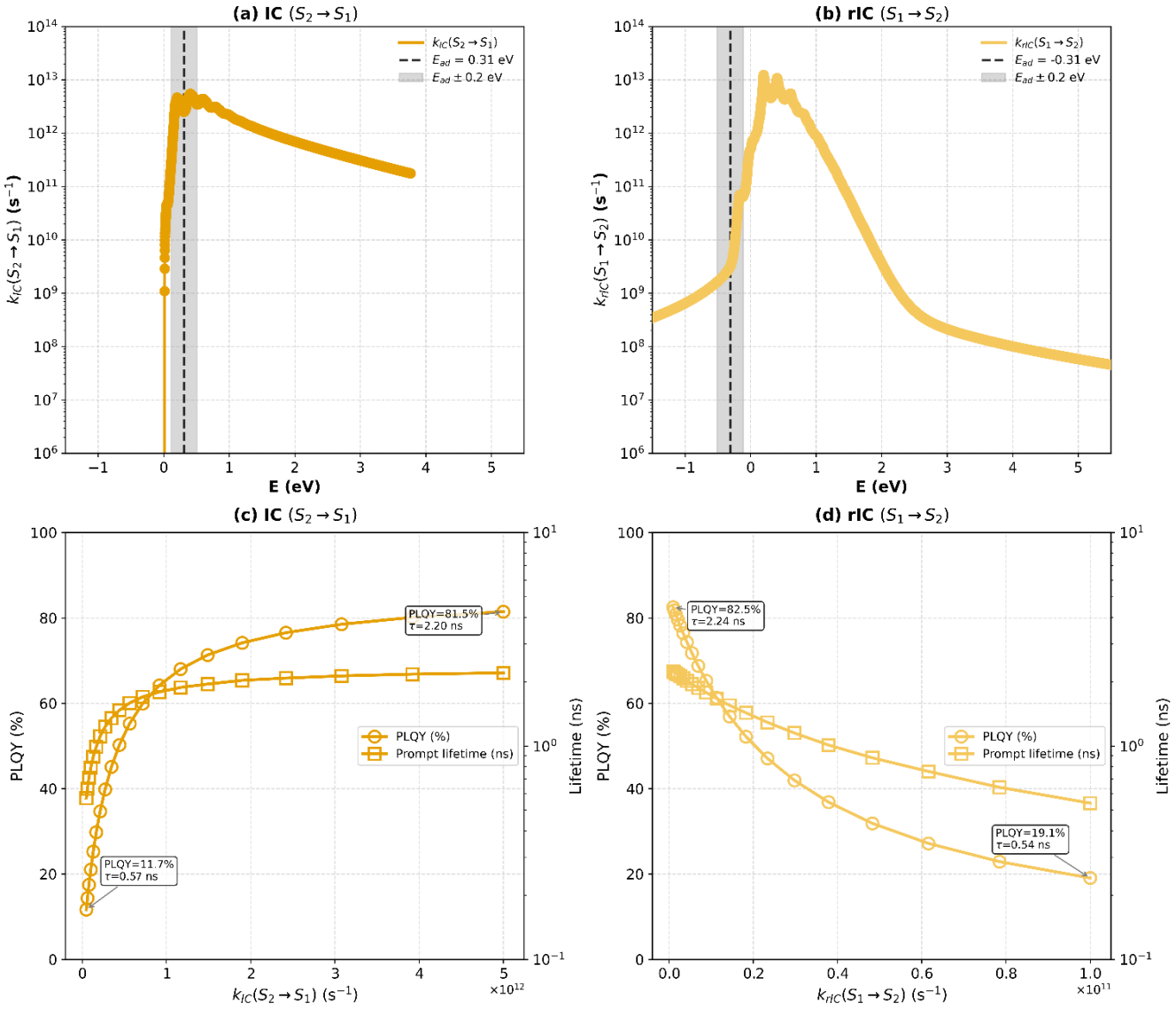

Figure S17. Dependencies of calculated rate constant on adiabatic energy gap for IC $S_2 \rightarrow S_1$ (a), rIC $S_1 \rightarrow S_2$ (b), and influences of IC $S_2 \rightarrow S_1$ (c), rIC $S_1 \rightarrow S_2$(d) rate constant on photoluminescence yield (PLQY) and lifetime in PPDs-1 using a five-state model.

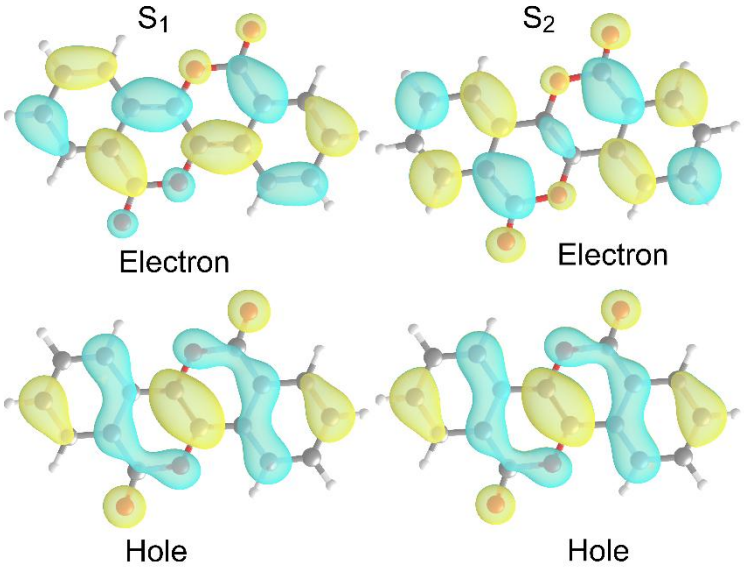

Figure S18. Natural transition orbitals (NTOs) of PPDs-1 at the S_1 and S_2 optimized geometries, calculated at the SCS-ADC(2) level of theory. Visualizations were generated using (a) VESTA[35] (isovalue = 0.026).

12. Simulated Excitation and Decay Kinetics Results Directly Generated by KinLuv

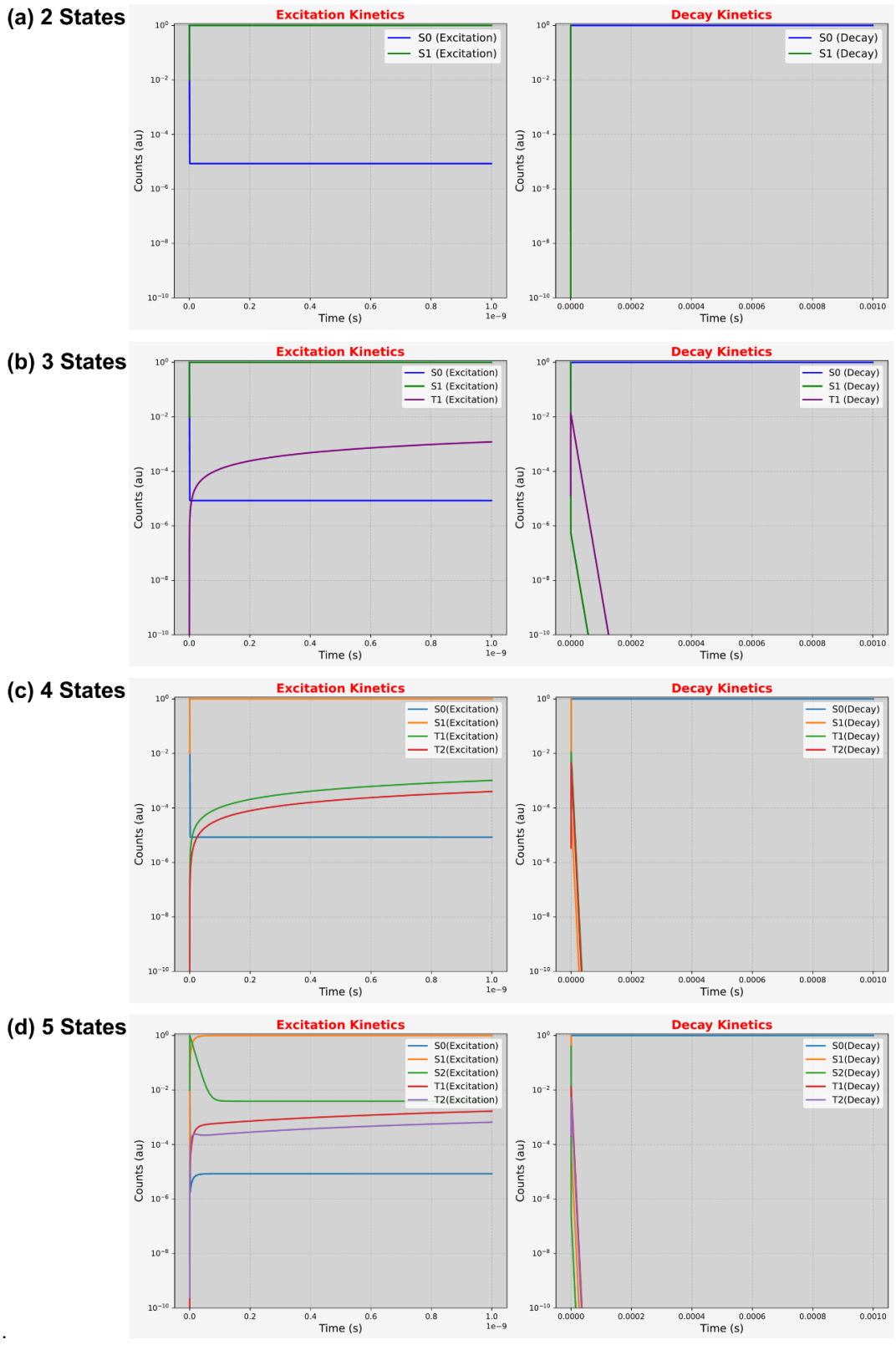

Figure S19. Excitation and decay plots generated by KinLuv for DOBNA based on (a) two-state, (b) three-state, (c) four-state, and (d) five-state kinetic models.

(a) 2 States

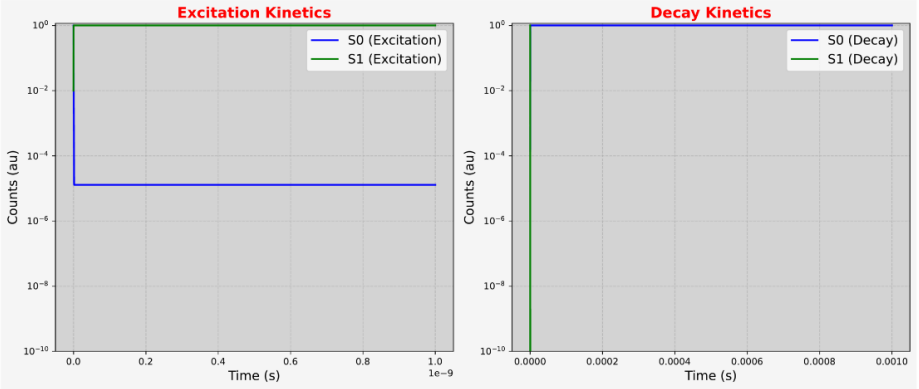

(b) 3 States

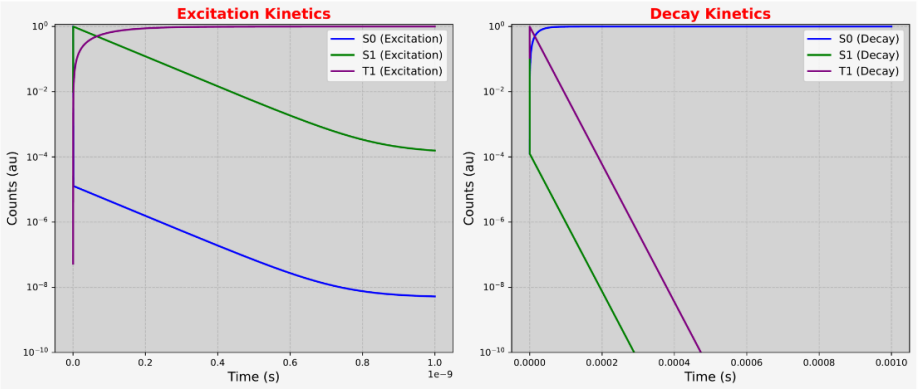

(c) 4 States

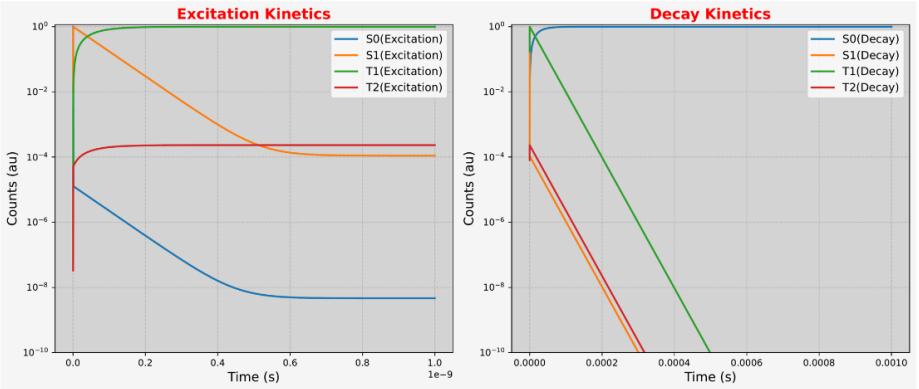

(d) 5 States

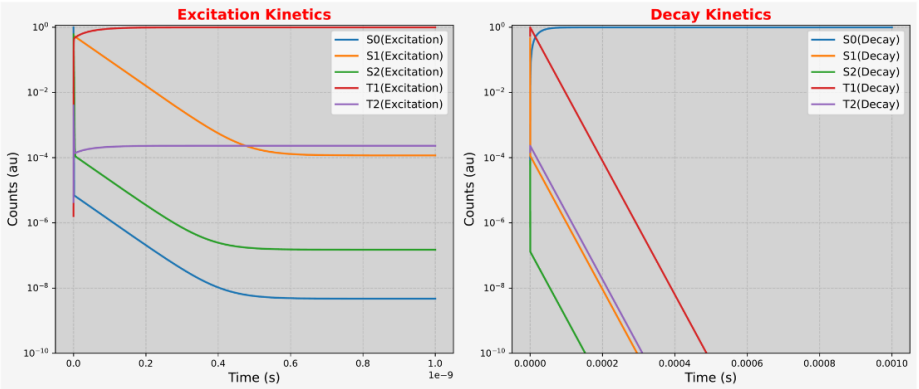

Figure S20. Excitation and decay plots generated by KinLuv for DiKTa based on (a) two-state, (b) three-state, (c) four-state, and (d) five-state kinetic models.

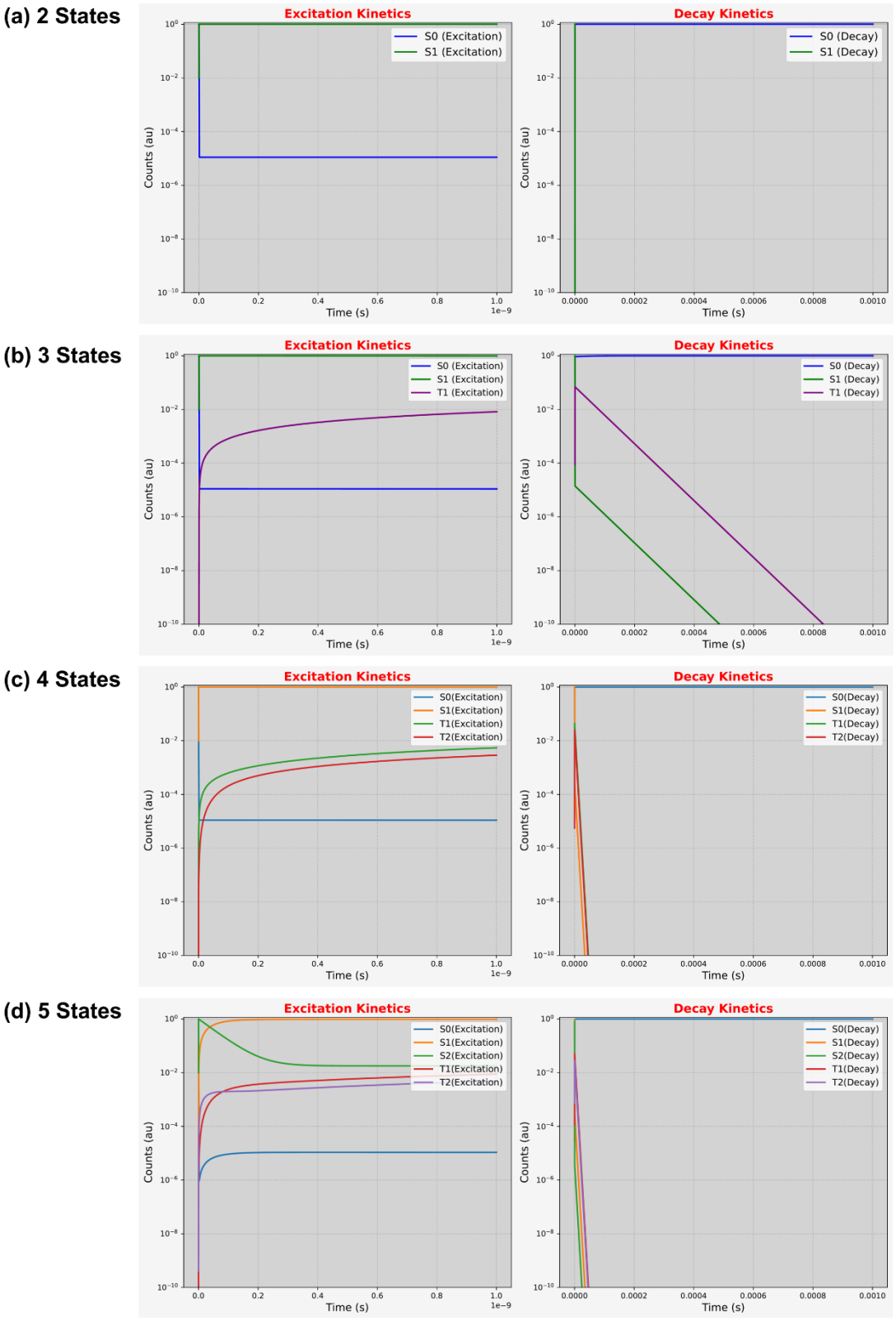

Figure S21. Excitation and decay plots generated by KinLuv for DABNA-1 based on (a) two-state, (b) three-state, (c) four-state, and (d) five-state kinetic models.

(a) 2 States

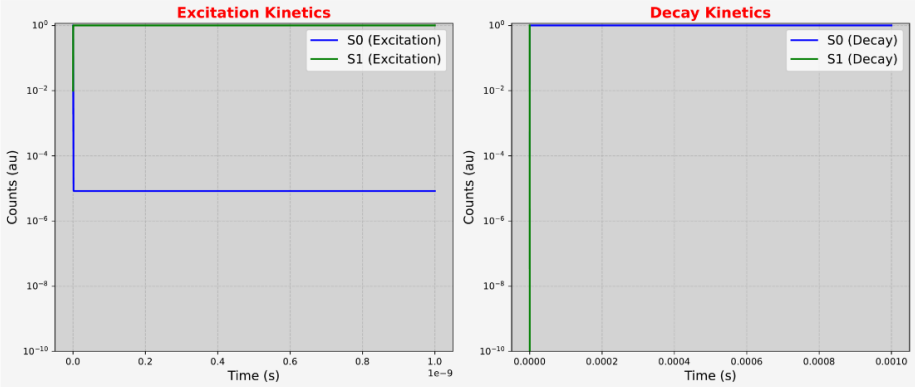

(b) 3 States

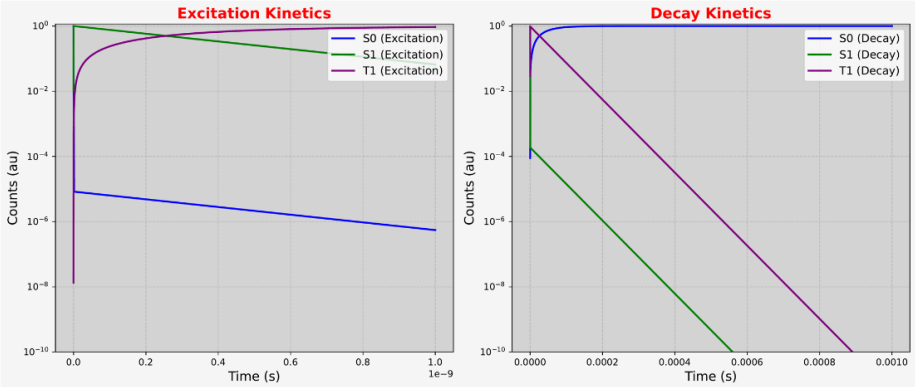

(c) 4 States

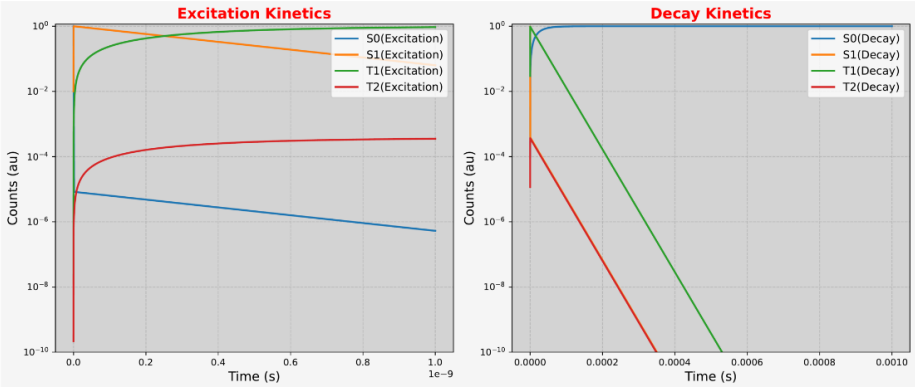

(d) 5 States

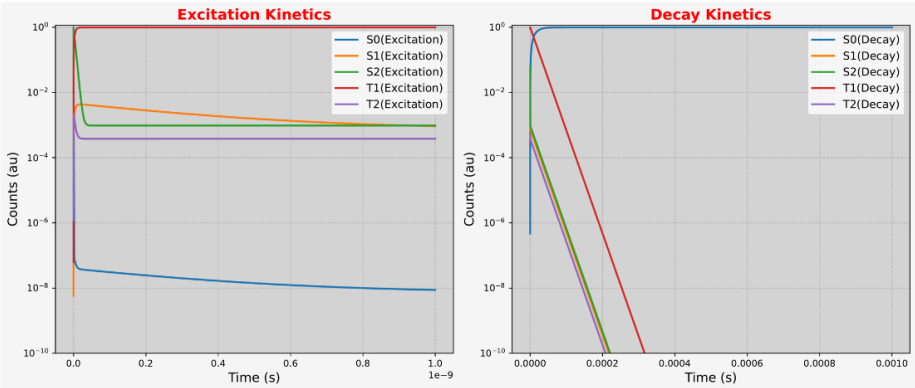

Figure S22. Excitation and decay plots generated by KinLuv for DQAO based on (a) two-state, (b) three-state, (c) four-state, and (d) five-state kinetic models.

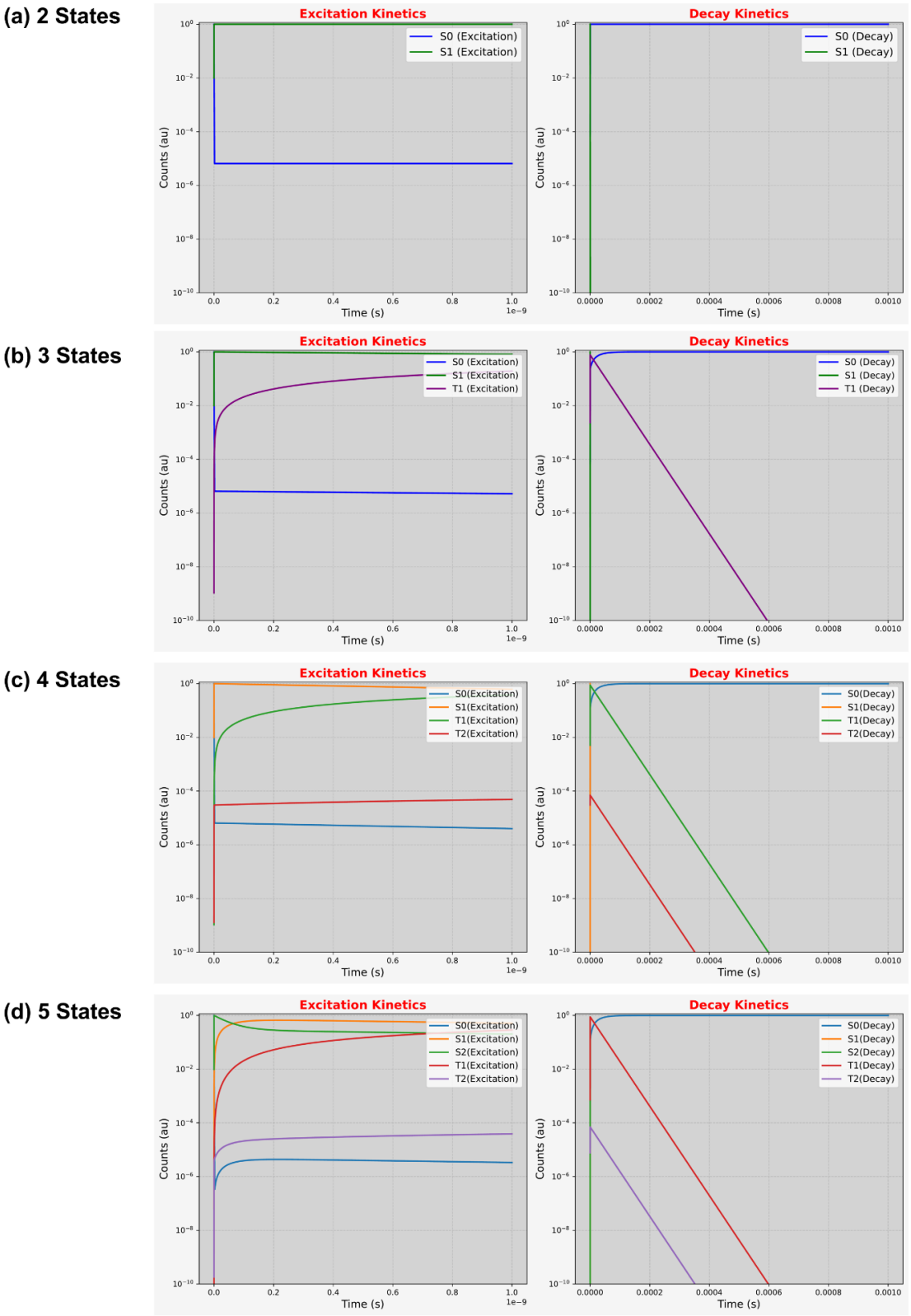

Figure S23. Excitation and decay plots generated by KinLuv for DBT based on (a) two-state, (b) three-state, (c) four-state, and (d) five-state kinetic models.

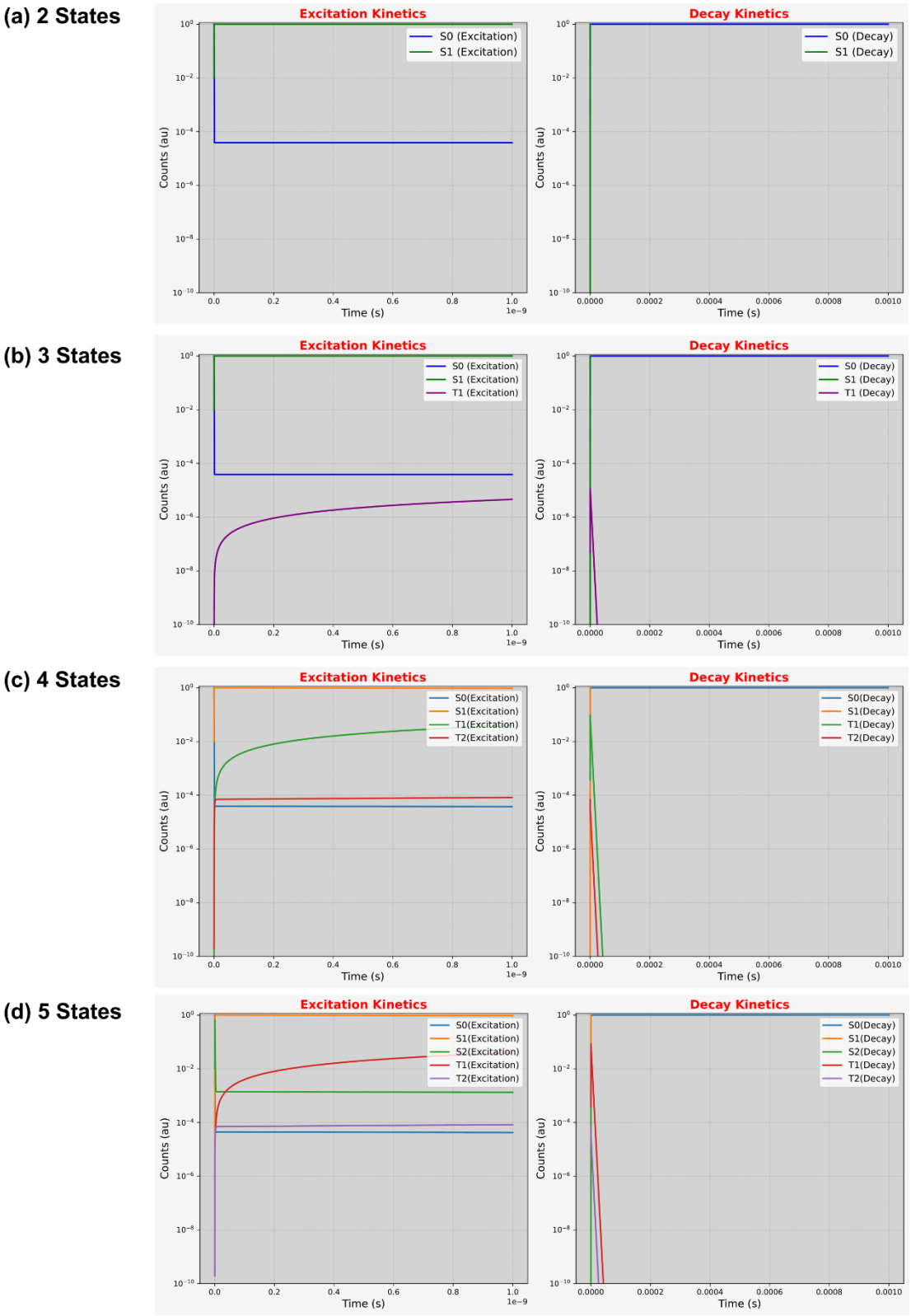

Figure S24. Excitation and decay plots generated by KinLuv for PPDs-1 based on (a) two-state, (b) three-state, (c) four-state, and (d) five-state kinetic models.

REFERENCE

1 M. T. Do Casal, K. Veys, M. H. E. Bousquet, D. Escudero and D. Jacquemin, *J. Phys. Chem. A*, 2023, **127**, 10033–10053.

2 P. Hohenberg and W. Kohn, *Phys. Rev.*, 1964, **136**, B864–B871.

3 W. Kohn and L. J. Sham, *Phys. Rev.*, 1965, **140**, A1133–A1138.

4 E. Runge and E. K. U. Gross, *Phys. Rev. Lett.*, 1984, **52**, 997–1000.

5 M. E. Casida, in *Recent Advances in Computational Chemistry*, WORLD SCIENTIFIC, 1995, vol. 1, pp. 155–192.

6 S. Hirata and M. Head-Gordon, *Chem. Phys. Lett.*, 1999, **314**, 291–299.

7 T. Yanai, D. P. Tew and N. C. Handy, *Chem. Phys. Lett.*, 2004, **393**, 51–57.

8 S. Grimme, J. Antony, S. Ehrlich and H. Krieg, *J. Chem. Phys.*, 2010, **132**, 154104.

9 A. V. Marenich, C. J. Cramer and D. G. Truhlar, *J. Phys. Chem. B*, 2009, **113**, 6378–6396.

10 M. J. Frisch, G. W. Trucks, H. B. Schlegel, G. E. Scuseria, M. A. Robb, J. R. Cheeseman, G. Scalmani, V. Barone, G. A. Petersson and H. Nakatsuji, *Gaussian 16*, Gaussian, Inc. Wallingford, CT, 2016.

11 A. Hellweg, S. A. Grün and C. Hättig, *Phys. Chem. Chem. Phys.*, 2008, **10**, 4119.

12 A. Dreuw and M. Wormit, *WIREs Comput. Mol. Sci.*, 2015, **5**, 82–95.

13 F. Weigend, M. Häser, H. Patzelt and R. Ahlrichs, *Chem. Phys. Lett.*, 1998, **294**, 143–152.

14 D. Jacquemin, I. Duchemin and X. Blase, *J. Chem. Theory Comput.*, 2015, **11**, 5340–5359.

15 D. Hall, J. C. Sancho-García, A. Pershin, G. Ricci, D. Beljonne, E. Zysman-Colman and Y. Olivier, *J. Chem. Theory Comput.*, 2022, **18**, 4903–4918.

16 M. T. Do Casal, Y. Badawy and D. Escudero, *J. Phys. Chem. C*, 2024, **128**, 18170–18181.

17 C. Hättig and F. Weigend, *J. Chem. Phys.*, 2000, **113**, 5154–5161.

18 TURBOMOLE GmbH, 2022.

19 Y. Shao, Z. Gan, E. Epifanovsky, A. T. B. Gilbert, M. Wormit, J. Kussmann, A. W. Lange, A. Behn, J. Deng, X. Feng, D. Ghosh, M. Goldey, P. R. Horn, L. D. Jacobson, I. Kaliman, R. Z. Khaliullin, T. Kuś, A. Landau, J. Liu, E. I. Proynov, Y. M. Rhee, R. M. Richard, M. A. Rohrdanz, R. P. Steele, E. J. Sundstrom, H. L. Woodcock, P. M. Zimmerman, D. Zuev, B. Albrecht, E. Alguire, B. Austin, G. J. O. Beran, Y. A. Bernard, E. Berquist, K. Brandhorst, K. B. Bravaya, S. T. Brown, D. Casanova, C.-M. Chang, Y. Chen, S. H. Chien, K. D. Closser, D. L. Crittenden, M. Diedenhofen, R. A. DiStasio, H. Do, A. D. Dutoi, R. G. Edgar, S. Fatehi, L. Fusti-Molnar, A. Ghysels, A. Golubeva-Zadorozhnaya, J. Gomes, M. W. D. Hanson-Heine, P. H. P. Harbach, A. W. Hauser, E. G. Hohenstein, Z. C. Holden, T.-C. Jagau, H. Ji, B. Kaduk, K. Khistyaev, J. Kim, J. Kim, R. A. King, P. Klunzinger, D. Kosenkov, T. Kowalczyk, C. M. Krauter, K. U. Lao, A. D. Laurent, K. V. Lawler, S. V. Levchenko, C. Y. Lin, F. Liu, E. Livshits, R. C. Lochan, A. Luenser, P. Manohar, S. F. Manzer, S.-P. Mao, N. Mardirossian, A. V. Marenich, S. A. Maurer, N. J. Mayhall, E. Neuscamman, C. M. Oana, R. Olivares-Amaya, D. P. O'Neill, J. A. Parkhill, T. M. Perrine, R. Peverati, A. Prociuk, D. R. Rehn, E. Rosta, N. J. Russ, S. M. Sharada, S. Sharma, D. W. Small, A. Sodt, T. Stein, D. Stück, Y.-C. Su, A. J. W. Thom, T. Tsuchimochi, V. Vanovschi, L. Vogt, O. Vydrov, T. Wang, M. A. Watson, J. Wenzel, A. White, C. F. Williams, J. Yang, S. Yeganeh, S. R. Yost, Z.-Q. You, I. Y. Zhang, X. Zhang, Y. Zhao, B. R. Brooks, G. K. L. Chan, D. M. Chipman, C. J. Cramer, W. A. Goddard, M. S. Gordon, W. J. Hehre, A. Klamt, H. F. Schaefer, M. W. Schmidt, C. D. Sherrill, D. G. Truhlar, A. Warshel, X. Xu, A. Aspuru-Guzik, R. Baer, A. T. Bell, N. A. Besley, J.-D. Chai, A. Dreuw, B. D. Dunietz, T. R. Furlani, S. R. Gwaltney, C.-P. Hsu, Y. Jung, J. Kong, D. S. Lambrecht, W. Liang, C. Ochsenfeld, V. A. Rassolov, L. V. Slipchenko, J. E. Subotnik, T. Van Voorhis, J. M. Herbert, A. I. Krylov, P. M. W. Gill and M. Head-Gordon, *Mol. Phys.*, 2015, **113**, 184–215.

20 F. Neese, *WIREs Comput. Mol. Sci.*, 2012, **2**, 73–78.

21 F. Neese, *WIREs Comput. Mol. Sci.*, 2022, **12**, e1606.

22 Y. Niu, Q. Peng, C. Deng, X. Gao and Z. Shuai, *J. Phys. Chem. A*, 2010, **114**, 7817–7831.

23 A. Humeniuk, M. Bužančić, J. Hoche, J. Cerezo, R. Mitrić, F. Santoro and V. Bonačić-Koutecký, *J. Chem. Phys.*, 2020, **152**, 054107.

24 J. Cerezo and F. Santoro, *J. Comput. Chem.*, 2023, **44**, 626–643.

25 P. A. M. Dirac, *Proc. R. Soc. Lond. Ser. Contain. Pap. Math. Phys. Character*, 1927, **114**, 243–265.

26 M. Born and R. Oppenheimer, *Ann. Phys.*, 1927, **389**, 457–484.

27 E. Condon, *Phys. Rev.*, 1926, **28**, 1182–1201.

28 Q. Peng, Y. Niu, C. Deng and Z. Shuai, *Chem. Phys.*, 2010, **370**, 215–222.

29 Z. Shuai and Q. Peng, *Phys. Rep.*, 2014, **537**, 123–156.

30 F. J. Avila Ferrer and F. Santoro, *Phys. Chem. Chem. Phys.*, 2012, **14**, 13549.

31 Q. Peng, Y. Yi, Z. Shuai and J. Shao, *J. Am. Chem. Soc.*, 2007, **129**, 9333–9339.

32 F. Santoro, A. Lami, R. Improta, J. Bloino and V. Barone, *J. Chem. Phys.*, 2008, **128**, 224311.

33 T. J. Penfold, E. Gindensperger, C. Daniel and C. M. Marian, *Chem. Rev.*, 2018, **118**, 6975–7025.

34 Q. Peng, Y. Yi, Z. Shuai and J. Shao, *J. Chem. Phys.*, 2007, **126**, 114302.

35 K. Momma and F. Izumi, *J. Appl. Crystallogr.*, 2011, **44**, 1272–1276.

36 T. Lu and F. Chen, *J. Comput. Chem.*, 2012, **33**, 580–592.

37 T. Lu, *J. Chem. Phys.*, 2024, **161**, 082503.